Chapter 5

CHAPTER 5

SEAWEED EXTRACT-BASED SOLID-STATE BIOPOLYMER ELECTROLYTE AND ITS APPLICATION TO ELECTROCHEMICAL STORAGE DEVICES

In the recent past, solid biopolymer electrolytes have gained more interest for the reason that they exhibit potential applications in electrochemical devices. Materials from natural sources found to attract many researchers as an alternative to synthetic polymers in energy storage. These solid bio-electrolytes possess several advantages like good mechanical - strength, leak-free, good electrode-electrolyte contact area, also facile and safe fabrication when compared to liquid electrolytes [1–3]. Natural polymeric materials provide comparable ionic conductivity and electrochemical stability to synthetic polymers and also offer cost economy and high flexibility. Environmentally benevolent biopolymers have been substantially explored to curtail ecological pollution. Hence, biopolymer membranes have been looked onto, as a potential candidate for the development of solid-state batteries. Multifold biopolymers like starch, cellulose acetate, chitosan, pectin, and carrageenan were studied to develop green membranes as solid electrolytes [4–6]. Materials from natural sources have received a surge of interest due to their anomalous properties like biodegradability, biocompatibility, and sustainability and also, they are renewable.

In the present research, an extract from seaweed, *Sargassum Muticum* has been investigated to prepare a bio-membrane. Seaweeds are rich in numerous polyphenolic compounds containing hydroxy groups and carboxyl groups in their structures which can act as the coordinating site for the ionic dopant [6]. Studies have revealed fucoxanthin [7–9], rutin, sulfated polysaccharides, alginates, and fucoidan [8,10]. Other constituents include fatty acids, essential amino acids, carbohydrates, polyphenols, and flavonoids [11–15]. This seaweed exhibits numerous benefits like antibacterial [8], antioxidant [7,16], and antimicrobial [17,18]. Unfortunately, the electrochemical properties because of these electroactive components haven't been investigated in the past. Hence, the use of *Sargassum Muticum* Extract (SME) using ethanol for the development of a solid bio-membrane electrolyte for battery fabrication is a novel approach. This has been affirmed by the GCMS analysis of the ethanol extract of SME and their interpretations are given in Figure 5.1 and Table 5.1

In order to improve the film-forming ability of SME, a non-toxic, biodegradable biopolymer, polyvinyl alcohol (PVA) is used as in our previous work [19]. The first-ever report

on bio-membrane from SME extract with 1g SME + 0.8g PVA (SMBP) as composition and its ionic conductivity was found to be $1.57 \pm 0.04 \times 10^{-6}$ S cm^{-1}.

5.1 Investigation of SME as solid bio-electrolyte for Mg-ion Battery

To improve the ionic conductivity of the prepared bio-membrane SMBP, a charge carrier $MgCl_2$ has been integrated into the bio-membrane composition. The low cost, abundance, low molecular weight, and safety make magnesium salts more attractive to be used as an ionic dopant and as anode material [20]. The ionic dissociation is easier for $MgCl_2$ due to its low lattice energy (2512 kJ/mol) compared to other magnesium salts, hence good solubility and enhanced conductivity making them a suitable choice as an ionic dopant in the present work [21]. This enabled the development of Mg – ion conducting SMBP bio-electrolytes for battery fabrication.

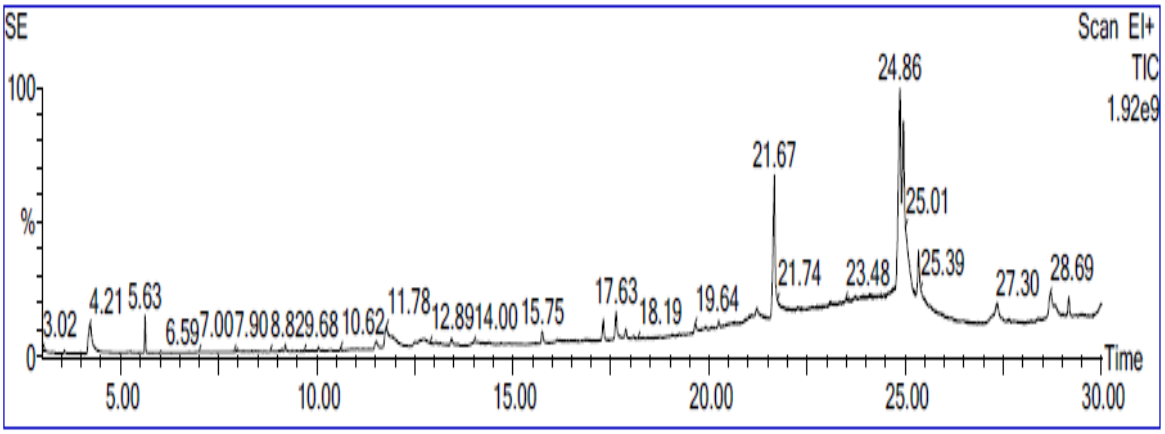

Figure 5.1: Chromatogram of the compounds in the *Sargassum Muticum* extract from GC – MS technique

5.1.1 Preparation of the bio-membrane and bio-electrolyte:

The bio-membrane has been prepared, using SME and PVA as mentioned in Chapter 3. The bio-membrane composition of 1g SME + 0.8g PVA (SMBP) possessing the highest ionic conductivity has been chosen for the bio-electrolyte preparation. The coalescence of the SMBP with $MgCl_2$ in different weight ratios as 0.5wt%, 0.6wt%, 0.7wt%, and 0.8wt% as represented in Table 1.4 are carried out by uniform blending for about 24hrs thus ensuring the proper mixing of the ionic dopant into the bio-membrane solution. Later the blend solution is

cast into the polypropylene petri dishes and is evaporated in a vacuum at 80°C for 24hrs and the developed bio-electrolyte as in Figure 5.2 are stored in a desiccator for further analysis.

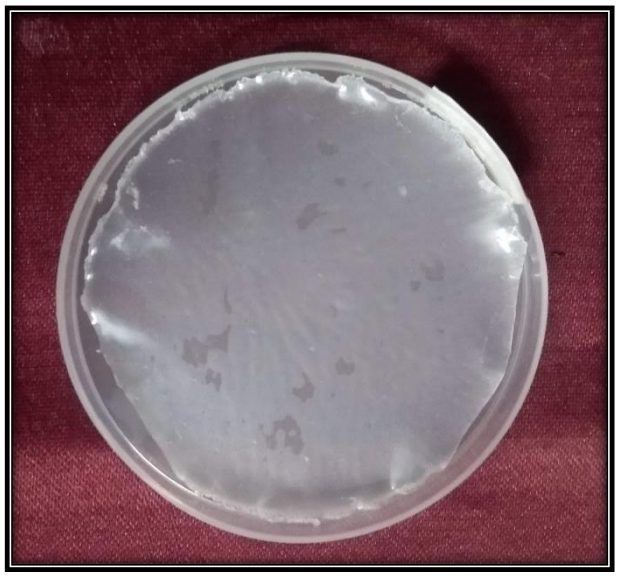

Figure 5.2: Biopolymer electrolyte membrane SMMC

Table 5.1: Interpretation of the compounds in the *Sargassum Muticum* extract from GC – MS technique

S.NO	RT	Compound Name	Area %
1	3.083	6-Ethoxy-6-methyl-2-cyclohexenone	0.529
2	3.239	4-Ethylbenzoic acid, cyclohexyl ester	0.261
3	3.574	Dimethyl sulfone	0.269
4	4.239	Glycerin	2.584
5	5.629	Propane, 1,1,3-triethoxy-	0.684
6	11.527	Dimethyl(bis[(2Z)-pent-2-en-1-yloxy])silane	0.486
7	11.782	3,7,11,15,19-Pentaoxa-2,20-disilaheneicosane, 2,2,20,20-tetramethyl-	3.193
8	12.507	2-Dimethyl(isopropyl)silyloxymethyltetrahydrofurane	0.266
9	12.632	d-Mannitol, 1,4-anhydro	0.246
10	13.438	Dodecanoic acid	0.289
11	14.098	Oxiraneundecanoic acid, 3-pentyl-, methyl ester, cis-	0.429
12	15.748	4-Phosphonobutyric acid	0.489

13	17.309	6-Hydroxy-4,4,7a-trimethyl-5,6,7,7a-tetrahydrobenzofuran-2(4H)-one	0.727
14	17.634	Tetradecanoic acid	0.994
15	19.645	Pentadecanoic acid	0.448
16	19.925	Actinomycin C2	0.262
17	20.245	4-(3,3-Dimethyl-but-1-ynyl)-4-hydroxy-2,6,6-trimethylcyclohex-2-enone	0.292
18	21.016	Bis(2-ethylhexyl) phthalate	0.257
19	21.226	Palmitoleic acid	1.198
20	21.666	n-Hexadecanoic acid	7.295
21	22.886	d-Gala-l-ido-octonic amide	0.237
22	23.186	Hexadecanoic acid, octadecyl ester	0.275
23	23.326	d-Mannose	0.662
24	23.507	Erucic acid	1.334
25	23.557	à-D-Glucopyranose, 4-O-á-D-galactopyranosyl-	0.654
26	23.747	Oleic Acid	1.862
27	23.937	à-D-Glucopyranose, 4-O-á-D-galactopyranosyl	2.13
28	23.937	d-Mannitol, 1-O-heptyl-	2.13
29	24.097	Estra-1,3,5(10)-trien-17á-ol	2.447
30	24.377	9,19-Cyclolanostan-24-one, 3-acetoxy-25-methoxy-	4.007
31	24.862	9,12-Octadecadienoic acid (Z,Z)-	16.994
32	24.952	Oleic Acid	17.865
33	25.337	Octadecanoic acid	7.825
34	27.353	Squalene	2.493
35	28.704	9,12-Octadecadienoic acid (Z,Z)-, 2-hydroxy-1-(hydroxymethyl)ethyl ester	2.858
36	29.164	Hexanedioic acid, bis(2-ethylhexyl) ester	0.604

5.1.2 X-ray Diffraction (XRD) Analysis

X-ray diffraction analysis has been performed to establish the effect of the ionic salt in the bio-electrolyte membrane on the crystalline or amorphous nature of the analyzed samples. Figure 5.3 and 5.4 shows the XRD spectra of SME and for the SMBP (1g SME + 0.8g PVA) membrane and Figure 5.5 displays the XRD pattern for the bio-electrolyte film SMBP with different wt% of $MgCl_2$ SMMC 0.5, SMMC 0.6, SMMC 0.7 and SMMC 0.8.

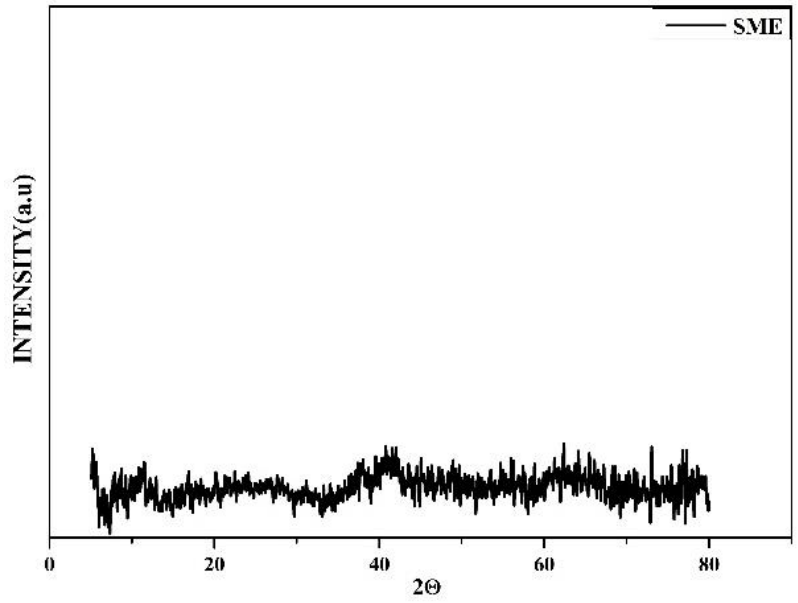

Figure 5.3: XRD pattern of SME

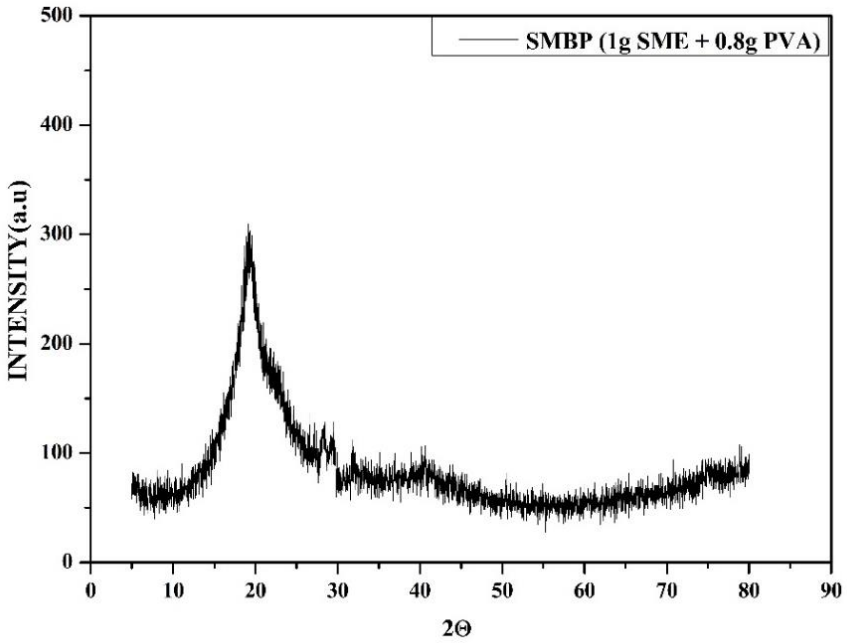

Figure 5.4: XRD pattern of SMBP (1g SME + 0.8g PVA)

The XRD pattern for SMBP includes a sharp diffraction peak at 19.1° and less intense peaks at 28.3°, and 30.1° are also observed. The sharp peak at 19.1° is due to the polyvinyl alcohol in the bio-membrane [22]. The small less intense peak at 28.3° and 30.1° may be due

to the components present in the SME [23] as represented in Figure 5.3. Upon incorporation of magnesium chloride salt into the prepared bio-membrane SMBP, the peaks found at 28.3°, and 30.1° in Figure 5.5 disappeared in all sample compositions of SMMC 0.5 to SMMC 0.8.

The broad peak centred at 21.5°, 22.1°, 23.5°, 24.5°, and 26.6° are observed along with a very small hump found at 39.5° for the compositions SMMC 0.5 and SMMC 0.6. but for SMMC 0.7 this small hump disappears and reappears in the composition SMMC 0.8. The X-ray pattern also implies that the broadness of the peak increases with an increase in the wt% of $MgCl_2$. The relative intensity of the peaks also decreases with an increase in the ionic dopant concentration until SMMC 0.7 after which the intensity increases as the charge carrier ions increase simultaneously. The increase in intensity is an indication of agglomeration of the $MgCl_2$ salt in the electrolyte membrane since the bio-membrane host was incapable to accommodate the ionic dopant [24, 25].

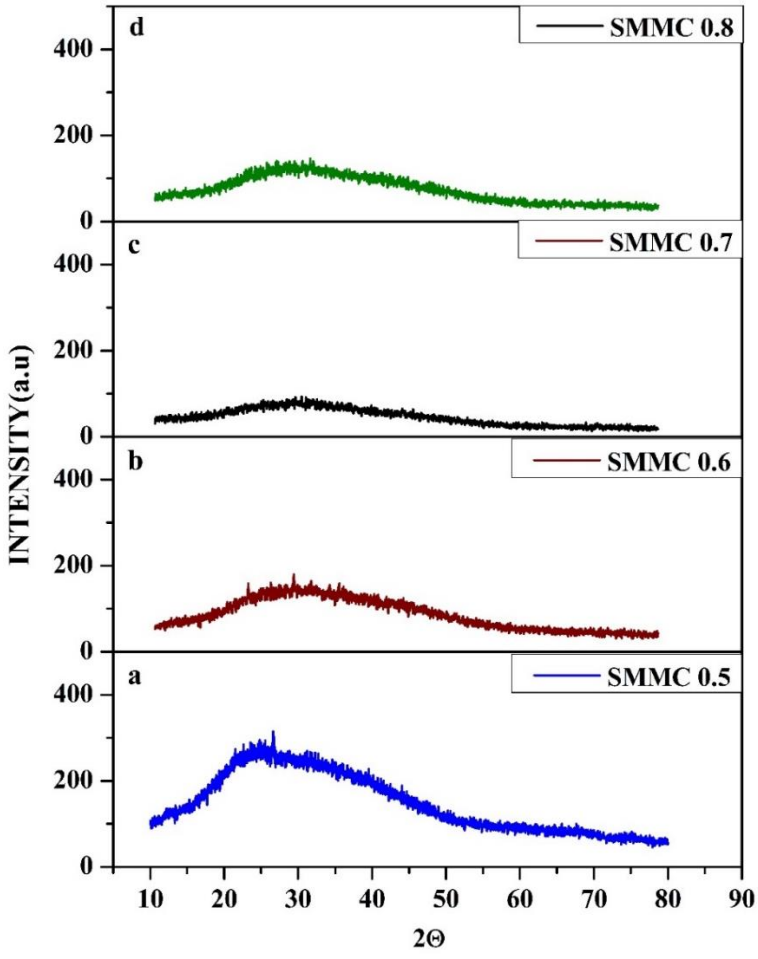

Figure 5.5: XRD pattern for the bio-electrolyte film SMBP with different wt% of $MgCl_2$

Table 5.2: Percentage of crystallinity for SMBP and SMMC 0.5, SMMC 0.6, SMMC 0.7, and SMMC 0.8 (different concentrations of $MgCl_2$)

Composition	Percentage of Crystallinity
1g SME + 0.8g PVA (SMBP)	59.36
1g SME + 0.8g PVA + 0.5wt% $MgCl_2$ (SMMC 0.5)	35.16
1g SME + 0.8g PVA + 0.6wt% $MgCl_2$ (SMMC 0.6)	18.49
1g SME + 0.8g PVA + 0.7wt% $MgCl_2$ (SMMC 0.7)	**12.81**
1g SME + 0.8g PVA + 0.8wt% $MgCl_2$ (SMMC 0.8)	25.49

The amorphous nature of the membrane increases with the increase in ionic dopant concentration and gets saturated at high ionic concentrations. The increase in the intensity of the peak for SMMC 0.8 is due to the increase in crystallinity as in Table 5.2 [26]. Thus, from Figure 5.5, it is evident that SMMC 0.7 with maximum ionic conductivity, has the maximum amorphous nature compared to other analyzed samples. The upsurge of the amorphous nature of the bio-electrolyte evokes a reduction in the energy barrier due to the segmental motion in the electrolyte membrane and thus increases the conductivity of the bio-electrolyte film [27–30].

5.1.3 Fourier Transform Infrared (FT-IR) Spectroscopy

The association and dissociation of the salt with the bio-membrane and the electrolyte system have been provided from the FTIR spectrum [31]. Figure 5.6 and 5.7 represent the FTIR spectrum for SME, ethanolic extract of *Sargassum Muticum*, and SMBP, the prepared bio-membrane film (1g SME + 0.8g PVA). Figure 5.8 illustrates the FTIR spectra for the electrolyte membranes SMMC 0.5 to SMMC 0.8.

For SME (Figure 5.6) the characteristic peaks observed are 3315 cm^{-1}, 2976 cm^{-1}, 1662 cm^{-1}, 1404 cm^{-1}, 1056 cm^{-1}, 837 cm^{-1}, and 690 $cm^{-1,}$ and their corresponding assignments are provided in Table 5.3. The ethanolic extract of *Sargassum Muticum* consists of carbohydrates, alkaloids, carboxylic acids [36] and phenolic compounds [37] as depicted in Figure 3.5.

Table 5.3: FTIR assignments for SME

Wavenumber (cm^{-1})	Assignments	References
3315	O – H Stretching	[32]
2976	C – H Stretching	[32]
1662	C=O stretching vibrations	[32]
1404	C – OH vibration of the carboxylate group	[32,33]
1056	C – O, C – C Stretching of the pyranose ring	[33,34]
837	Anomeric C – H deformation	[35]

Table 5.4: Peak position and vibrational Assignments of SMBP and $MgCl_2$ incorporated bio-electrolytes

Assignments	SMBP (cm^{-1})	SMMC 0.5 (cm^{-1})	SMMC 0.6 (cm^{-1})	SMMC 0.7 (cm^{-1})	SMMC 0.8 (cm^{-1})
H-bonded –OH	3392	3304	3313	3329	3305
–CH stretching	2902	2918	2927	2939	2954
C=O stretching vibrations	1703	1639	1637	1645	1654
C–OH vibration of the carboxylate group	1425	1429	1431	1433	1433
Asymmetric $–CH_2$ stretching	1253	1257	1259	1265	1257
C – O stretching of an acetyl group	1068	1083	1085	1093	1087

A characteristic band at 3315 cm^{-1} and a weak band at 2976 cm^{-1} for SME may be assigned to O–H stretching and C–H stretching vibrations respectively [38]. The presence of two absorption signals at 1662 cm^{-1} and at 1404 cm^{-1} may be due to the asymmetric and symmetric stretching vibrations of the carboxylate groups in the *Sargassum Muticum* Extract (SME) [32–34]. The presence of a band at 1056 cm^{-1} corresponds to the C – O and C – C

stretching of the pyranose rings in SME [33]. Also, a peak observed at 837 cm^{-1} is due to the anomeric C-H deformation in polysaccharides [23, 39].

A characteristic band due to O–H stretching has been observed at 3392 cm^{-1} for SMBP (1g SME + 0.8g PVA) membrane after being blended with PVA (Figure 5.7). This band gets shifted to lower wavenumbers at 3304 cm^{-1}, 3313 cm^{-1}, 3329 cm^{-1}, and 3305 cm^{-1} for $MgCl_2$ incorporated bio-electrolyte films SMMC 0.5 to SMMC 0.8 as in Table 5.4 which suggests the interaction of the bio-membrane with the added salt [40, 41]. Generally, a band shift shows the interaction of the host with the salt. Here the shift in the hydroxyl band with increasing salt concentration proves that Mg^{2+}-ion coordinates with the negatively charged oxygen atoms of the hydroxyl group [42]. A small and weak band at 2902 cm^{-1} for SMBP is shifted to 2918 cm^{-1}, 2927 cm^{-1}, 2939 cm^{-1}, and 2954 cm^{-1} respectively for salt-induced electrolyte systems [43]. The peak corresponding to C=O stretching vibrations has been observed at 1703 cm^{-1} for SMBP, whereas this peak shifts to 1639 cm^{-1}, 1637 cm^{-1}, 1645 cm^{-1}, and 1654 cm^{-1} respectively for the salt-doped electrolyte membranes.

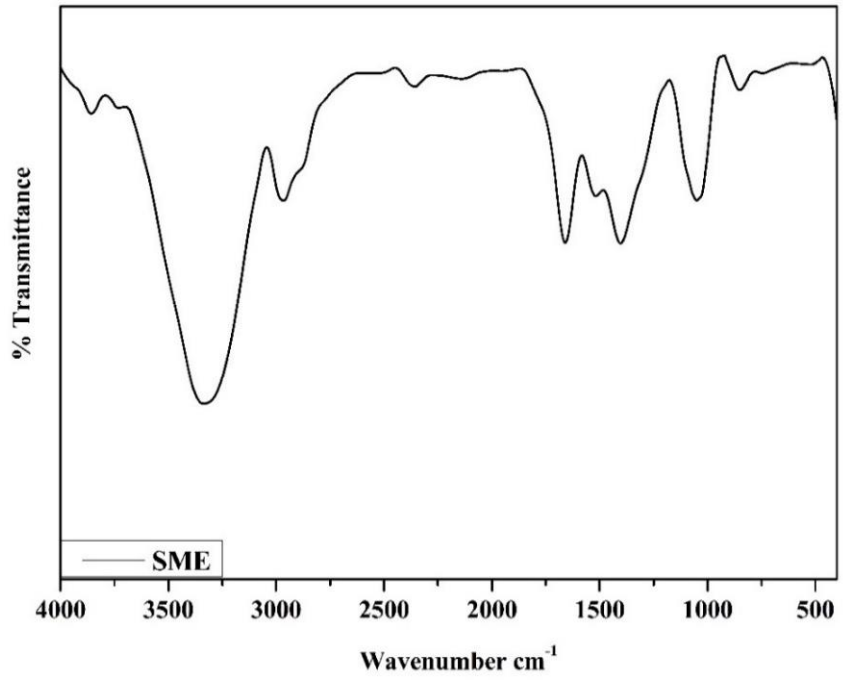

Figure 5.6: FTIR spectra of Sargassum Muticum Extract (SME)

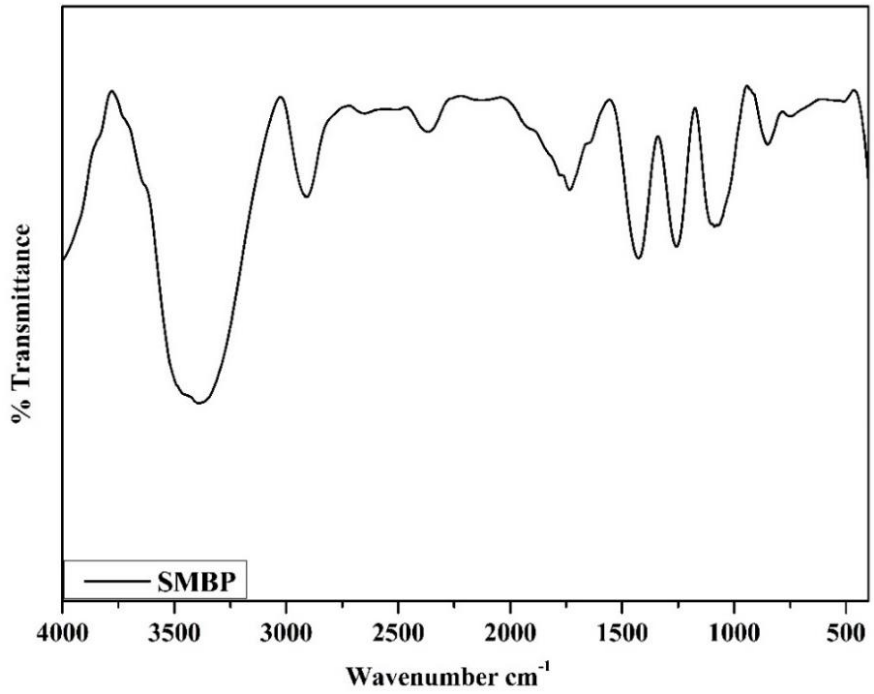

Figure 5.7: FTIR spectra of SMBP (1g SME +0.8g PVA)

In addition, a peak observed at 1425 cm^{-1} in SMBP is shifted to 1429 cm^{-1}, 1431 cm^{-1}, 1433 cm^{-1}, and 1433 cm^{-1} for the salt-complexed electrolyte films. The absorption bands around 1253-1257 cm^{-1} for SMBP and SMMC 0.5 to SMMC 0.8 films may be assigned to asymmetric – CH_2 groups twisting vibrations [44, 45]. The bands at 1083 - 1093 cm^{-1} have been attributed to C – O stretching of acetyl groups present in the PVA backbone for SMBP and other bio-electrolyte films SMMC 0.5 to SMMC 0.8 respectively [45, 46]. Hence the spectral analysis reveals the changes in the structural backbone of the bio-membrane backbone before and after blending PVA and the increase in addition of the ionic dopant.

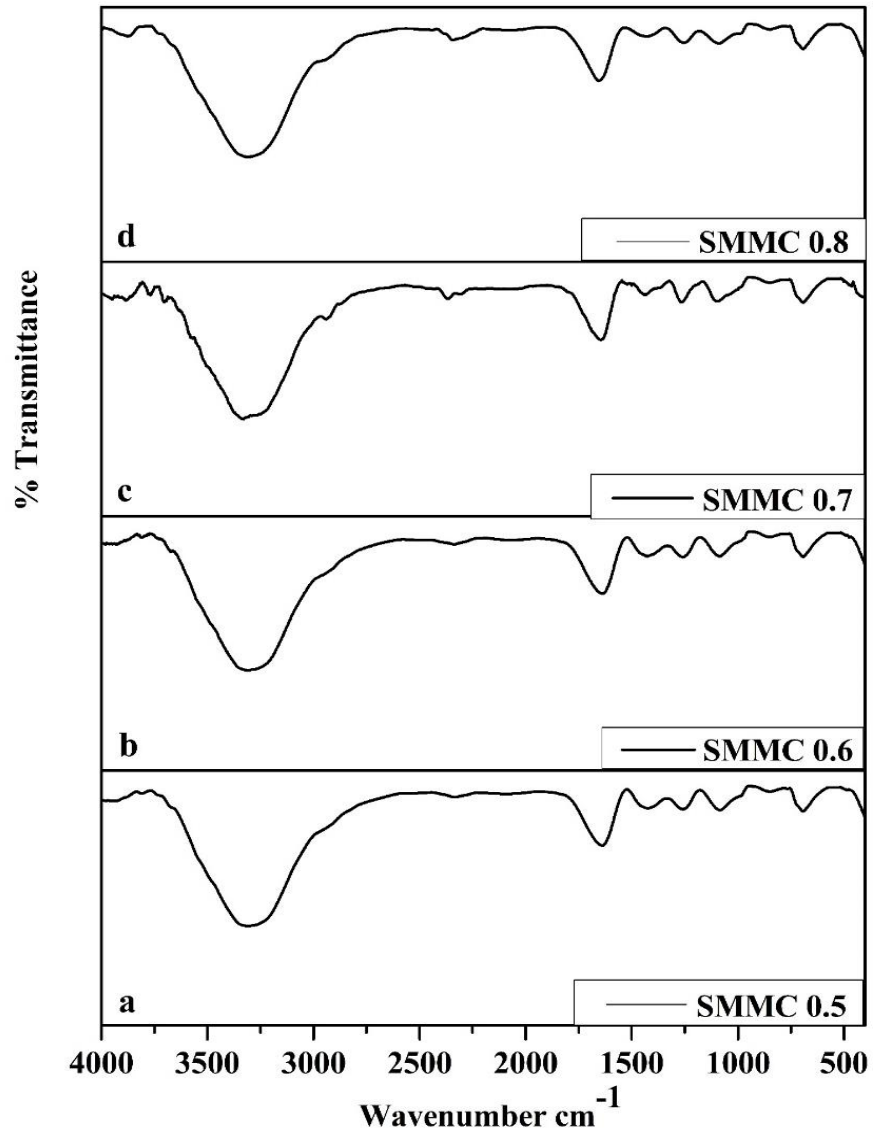

Figure 5.8: FTIR spectra of SMMC 0.5 (a), SMMC 0.6 (b), SMMC 0.7 (c), SMMC 0.8 (d)

5.1.4 Differential Scanning Calorimetry (DSC)

The thermal properties of the prepared bio-membrane and salt-doped electrolyte membranes have been studied using a powerful technique, differential scanning calorimetry. Figure 5.9 and 5.10 illustrates the thermogram of SME, SMBP (1g SME + 0.8g PVA) and Figure 5.11 shows the thermogram for SMMC 0.5, SMMC 0.6, SMMC 0.7, and SMMC 0.8. The DSC thermogram for SME exhibits two endothermic peaks at 58.7°C and 87.8°C which

may be due to the evaporation of moisture content in *Sargassum Muticum* [47]. The thermogram of the SMBP membrane shows a T_g value at 60.0°C. This increase in the T_g value of the SMBP film may be due to the presence of PVA, whose Tg value is 70°C [19].

With the addition of 0.5wt% $MgCl_2$ to the biopolymer SMBP, the T_g values further drop to 56.0°C due to the plasticizing effect of the added salt [48]. Further increase in the concentration of the magnesium chloride to 0.6wt% $MgCl_2$ and 0.7wt% $MgCl_2$ the glass transition temperature also decreases to 50.7°C and 45.4°C. The inclusion of salt in the bio-membrane fosters the rubbery nature which in turn contributes to the improvement of the amorphous nature of the electrolyte membrane thus leading to the lowering of the T_g value of the bio-electrolyte films. An increase in amorphous nature results in the enhancement of movement of Mg^{2+} ions [49]. The glass transition temperature decreases until 0.7wt% $MgCl_2$ and increases to 56.6°C when 0.8wt% $MgCl_2$ is added to the biopolymer matrix which is attributed to the formation of an ionic cluster that hinders the mobility of Mg^{2+} ions.

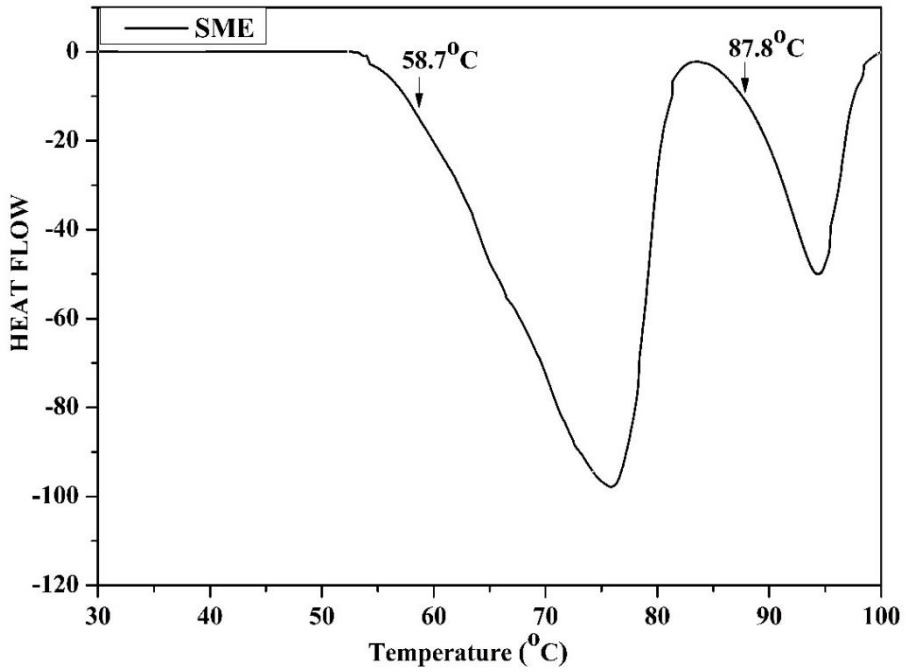

Figure 5.9: DSC thermogram of SME

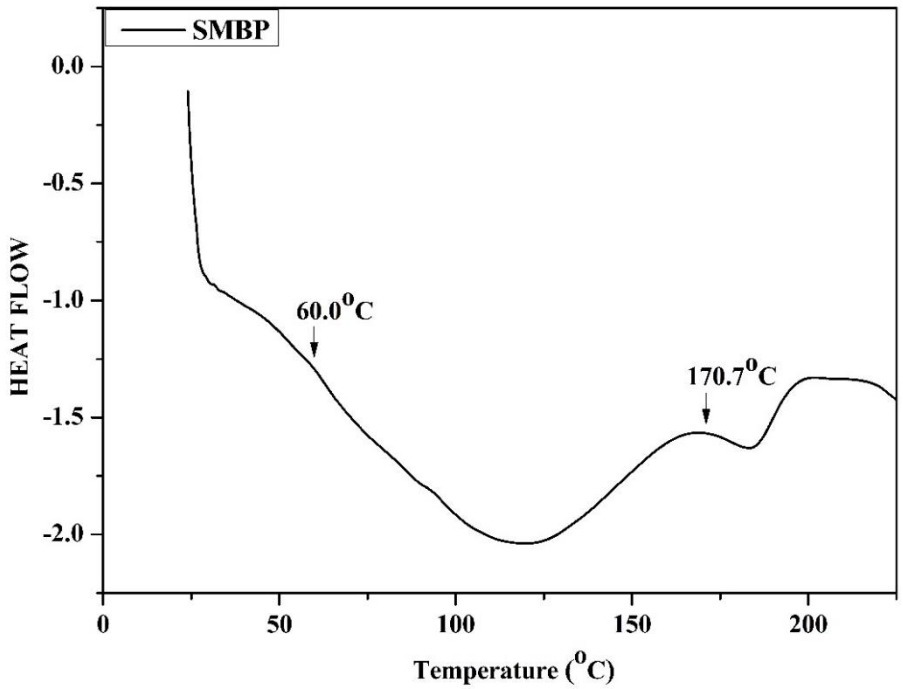

Figure 5.10: DSC thermogram of SMBP (1g SME + 0.8g PVA)

The addition of a higher concentration of salt results in agglomeration of the ionic dopant in the polymer matrix [49]. Another endothermic peak is observed at 170.7°C indicating the melting temperature of the SMBP membrane. In salt incorporated systems SMMC 0.5 to SMMC 0.8, this melting temperature is found at 168.5°C, 164.7°C, 160.9°C, and 155.2°C respectively. Similar results have been obtained for Mahalakshmi et al [50] for the composition 40%CA:60%Mg $(ClO_4)_2$ biopolymer membrane and Ponraj et al for the composition 70 wt% poly (VdCl-*co*-AN-*co*-MMA):30 wt% $MgCl_2$:0.3 wt% SN [51].

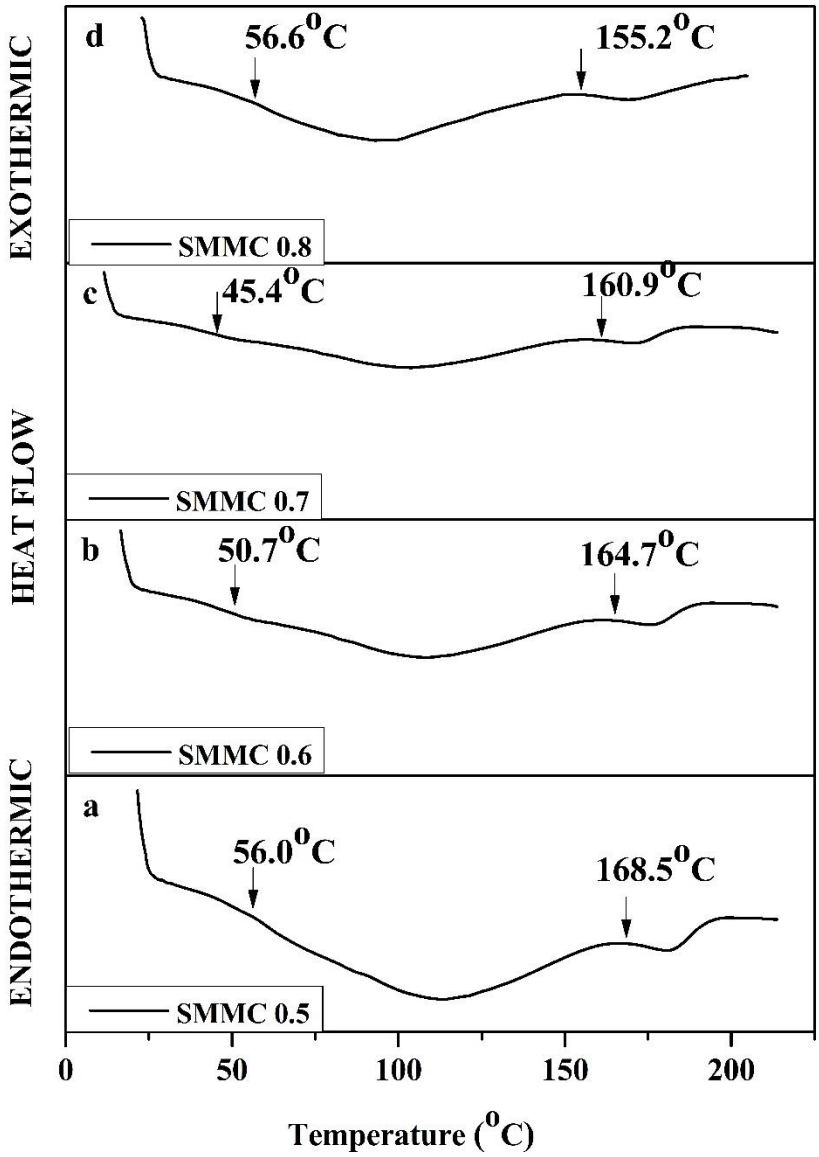

Figure 5.11: DSC thermogram of SMMC 0.5 (a), SMMC 0.6 (b), SMMC 0.7 (c), SMMC 0.8 (d)

5.1.5 Linear Sweep Voltammetry (LSV)

The electrochemical stability window for the highest conducting bio-electrolyte has been obtained from the LSV study as in the Figure 5.12.

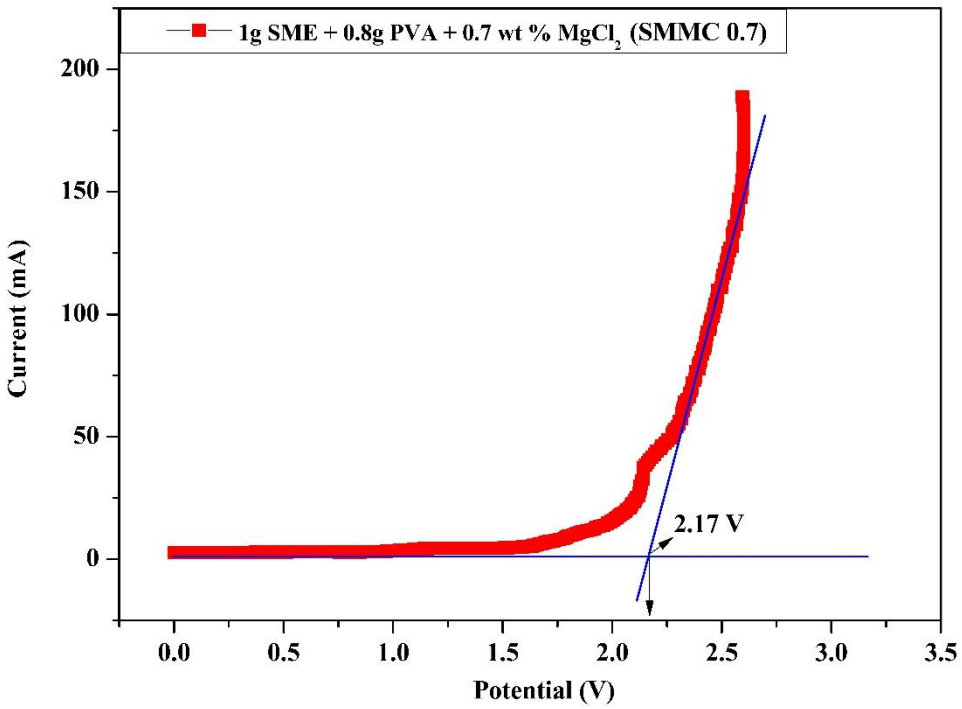

Figure 5.12: LSV plot for the highest proton conducting SMMC 0.7 bio-electrolyte.

The prepared bio-electrolyte undergoes electrochemical reaction and hence starts to degrade during the potential range and this potential has been inferred to as the decomposition potential for the bio-electrolyte. In the present work, the decomposition starts to take place after 1.6 V and after which the current increases abruptly. Thus, the electrochemical stability window for SMMC 0.7 has been found to be 2.17 V. This makes this bio-electrolyte to be employed for its application in electrochemical devices. Hamsan et al.,[21] reported an electrode potential stability window of 1.83V for Chitosan- $MgCl_2$- Glycerol system. Sangeetha et.al., obtained a potential window of 1.94 V for the $MgCl_2$ doped K-carrageenan system [58].

5.1.6 Transfer number measurement analysis (TNM)

One of the reliable parameters, to apply the prepared bio-electrolytes suitable for battery purposes, is transference number analysis. In this context, Wagner's polarization technique [52] has been employed to assess the ionic transference number of the ionic species in the electrolyte. In this technique, a dc voltage of 1.5V is introduced across the electrolyte of the highest conducting electrolyte membrane packed between the stainless-steel electrodes (SS|1g

SME + 0.8g PVA + 0.7wt% $MgCl_2$|SS), and the resultant current is observed as a function of time.

After polarization, the initial current decreases due to the flow of mobile ions, and a residual current remains after the current lays off, which is termed the final current as depicted in Figure 5.13. The transference number can be calculated from the equation (3.3) and (3.4) as discussed in Chapter 3. I_i, I_f are the initial and final current which is obtained from Figure 5.13. The maximum transference value is derived from the above equation as 0.97 for the highest conducting composition 1g SME + 0.8g PVA + 0.7wt% $MgCl_2$. This substantiates that the conductivity of the bio-membrane electrolyte system is dominated by the mobility of the ions.

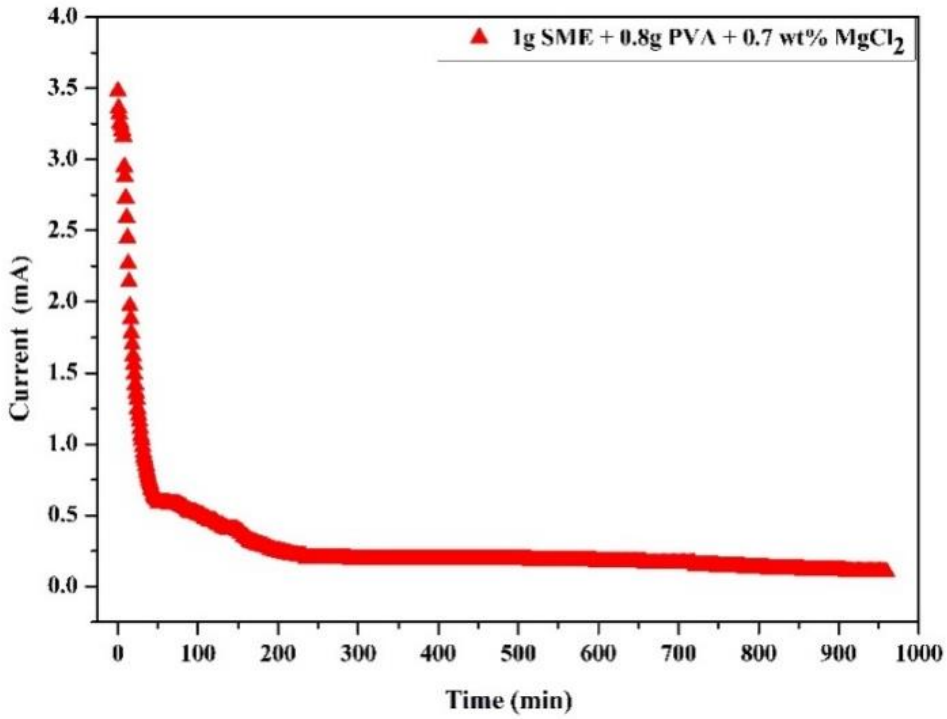

Figure 5.13: Polarisation cure Vs Time of the cell for the highest conducting SMMC 0.7 bio-electrolyte

5.1.7 AC Impedance spectroscopy

Impedance spectroscopy is a significant tool to assess the electrical properties of polymer electrolytes. The Cole-Cole plot of the prepared bio-membranes using 1g of SME and varying concentrations of PVA from 0.4g to 1g are shown in Figure 3.7. Figure 3.6 depicts the

Cole-Cole plot for the optimized bio-membrane, 1g SME + 0.8g PVA along with the equivalent circuit. The plot shows a depressed semicircle in the high-frequency region due to the bulk resistance of the bio-membrane film and an inclined spike due to the electrode/electrolyte interface in the low-frequency region [53]. The ionic conductivity values of all the prepared bio-membranes are presented in Table 3.2. Figure 5.14 shows the Cole-Cole plot for the optimized bio-membrane SMBP and various concentrations of $MgCl_2$ incorporated membranes SMMC 0.5, SMMC 0.6, SMMC 0.7, and SMMC 0.8. In the case of the prepared bio-membranes, the depressed semicircle has completely disappeared with the addition of varying concentrations of the salt as in SMMC 0.5 to SMMC 0.8 and only a tilted spike exists. This explains the predominance of resistive components alone in the prepared electrolyte membranes [54].

The disappearance of the semicircle at the high-frequency region may be due to the transfer of entire ions to the electrodes [21]. The corresponding equivalent circuit is provided in Figure 5.14. The ionic conductivity of the blend bio-membrane samples has been evaluated from equation (3.5) in Chapter 3. The bulk resistance for all the prepared samples is computed from the EQ software established by B.A. Boukamp [55–57]. The calculated ionic conductivity for all the prepared samples is tabulated in Table 5.5. It is evident from the table that SMBP has the highest R_b value due to the absence of charge carrier ion and later, with the increase in addition of the ionic dopant, the bulk resistance R_b value decreased from SMMC 0.5 to SMMC 0.7 respectively.

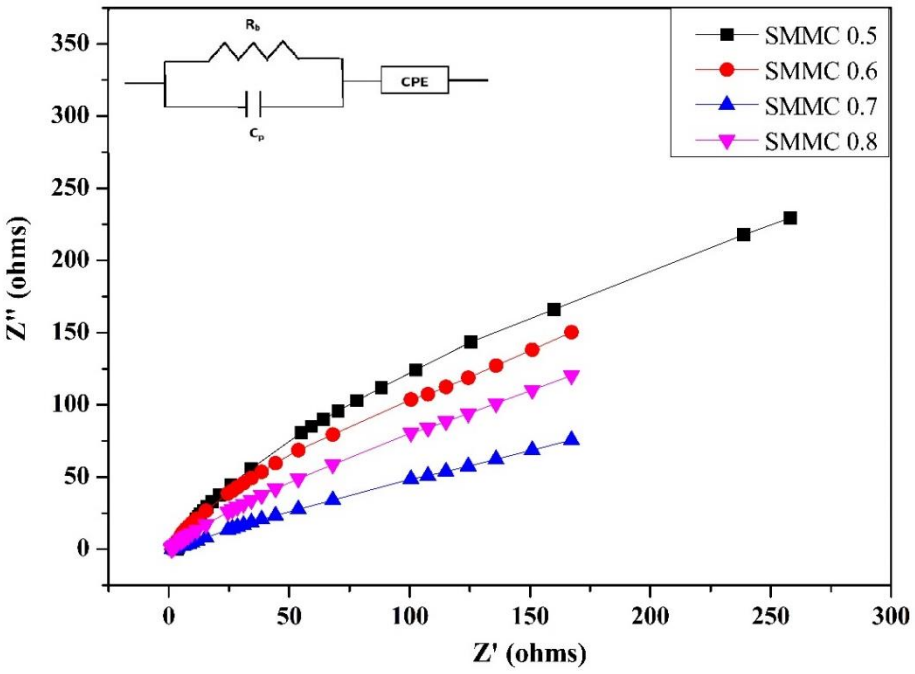

Figure 5.14: Nyquist plot for the prepared bio-electrolytes SMMC 0.5, SMMC 0.6, SMMC 0.7 and SMMC 0.8 at 303K

The Mg- ion-conducting film (SMMC 0.7) with the lowest R_b value has the maximum ionic conductivity which is 2.22 × 10^{-3} Scm^{-1} at 303K and beyond this concentration, conductivity decreases. The improved ionic conductivity is associated with increased ionic mobility within the electrolyte membranes [58] and an enhanced amorphous nature [53]. The increased amorphic nature promotes the facile transportation of charge carriers which in turn maximizes the ionic conductivity. The drop in the conductivity beyond the optimized composition for SMMC 0.8 is attributed to the aggregation of the carrier ions and ion pair formation which inhibits the ionic mobility [49, 59]. Comparable results of ionic conductivity 1.01×10^{-3} Scm^{-1} were obtained for the biopolymer composition 92.5PVA:7.5PAN:0.5 m.m.% $MgCl_2$ for Manjuladevi et al [60] and Adlin Helen et al obtained an ionic conductivity of 4.6139 × 10^{-4} Scm^{-1} for Chitosan with 70 wt% of $MgCl_2$ [41]. Mangalam et al reported DC conductivity of 1.1 × 10^{-4} Scm^{-1} for 50 m% PVA-50 m% PVP:25 m% Mg $(ClO_4)_2$ [61] and Sangeetha et al, 2.18 × 10^{-3} S cm^{-1} for 0.6 M wt% of magnesium perchlorate with κ-Carrageenan [62].

Table 5.5: Ionic conductivity (σ) values of the prepared bio-membrane and electrolytes at 303K

Composition	**σ (S cm^{-1})**	**R_b (Ω)**
1g SME + 0.8g PVA	1.57×10^{-6}	6200
1g SME + 0.8g PVA + 0.5wt% $MgCl_2$ (SMMC 0.5)	3.34×10^{-3}	6.13
1g SME + 0.8g PVA + 0.6wt% $MgCl_2$ (SMMC 0.6)	3.99×10^{-3}	4.12
1g SME + 0.8g PVA + 0.7wt% $MgCl_2$ (SMMC 0.7)	**2.22×10^{-3}**	**2.74**
1g SME + 0.8g PVA + 0.8wt% $MgCl_2$ (SMMC 0.8)	7.94×10^{-4}	13.87

5.2 Investigation of SME as solid bio-electrolyte for Li-Ion Battery

The *Sargassum Muticum* biomass has been extracted with ethanol and the extract SME has been blended with the polyvinyl alcohol to prepare the optimized blend SMBP (1g SME + 0.8g PVA). In this section, we are discussing the preparation of the lithium chloride incorporated bio-electrolyte and its characterization.

5.2.1 Preparation of the Sargassum bio-electrolyte for Li-ion Battery

The bio-polymer membrane SMBP has been synthesized as discussed in Chapter 3 and by dispersing polyvinyl alcohol (PVA) and *Sargassum Muticum* Extract (SME). From the Nyquist plots the appropriate composition of the bio-polymer membrane as in Figure 3.6 is chosen and optimized from the respective ionic conductivity values. Thus, the optimized ratio has been 1g SME + 0.8g PVA with a maximum conductivity of 1.57×10^{-6} Scm^{-1}. The bio-electrolyte using the charge carrier ions as lithium chloride has been prepared with the addition of 0.4wt%, 0.5wt%, 0.6 wt%, and 0.7wt% of LiCl to the SMBP composition by solution casting technique as in Figure 5.15. The designations are represented in Table 1.5 and the prepared Sargassum bio-electrolytes are characterized.

Figure 5.15: Biopolymer electrolyte membrane SMLC

5.2.2 X-ray Diffraction (XRD) Analysis

The amorphous /crystalline nature of the samples SMLC 0.4, SMLC 0.5, SMLC 0.6, and SMLC 0.7 are analyzed by X-ray diffraction technique and are illustrated in Figure 5.16. The diffraction spectrum for the corresponding bio-polymer membrane SMBP (1g SME + 0.8g PVA) has been discussed initially in this chapter in Figure 5.3. The XRD pattern for the SMBP membrane consisted of a sharp diffraction peak at 19.1° and less intense peaks observed at 28.3°, and 30.1°. The sharp peak at 19.1° has been attributed to PVA used for blending along with the sargassum extract in the bio-membrane SMBP [22] and the small less intense peaks at 28.3°, 30.1 has been accounted for the components present in the SME [38] as represented in Figure 5.3. The degree of crystallinity for the samples has been evaluated using the formula in the equation (3.2) as provided in Chapter 3 and the values are listed in Table 5.6.

The integration of the ionic dopant lithium chloride with the bio-membrane SMBP has made the peaks to be less prominent in SMLC 0.4, SMLC 0.5, and SMLC 0.6. It is obvious that with the increase in the concentration of the LiCl salt in the SMBP has reduced the peak intensity along with the widening of the peak. The diffraction peak observed at 19.1° and 28.3°, 30.1° in SMBP has broadened to give an amorphous peak at 26.6° in SMLC 0.4 which is observed at a relatively low intensity for SMLC 0.5 and SMLC 0.6. This reduction of relative intensity and broadening of Bragg's peak is explained by the distortion of the ordered phase of the molecules in the biopolymer membrane SMBP which agrees with Hodge et al.,[63]. The

attainment of the amorphous peak with an increase in dopant concentration is the maximum for SMLC 0.6 membrane thus leading to the flexibility of the membrane due to the segmental motion of the host matrix of SMBP [64, 65]. The amorphous phase of the membrane hence helps in easy ionic diffusion of the dopant ions through the membrane and thereby enhancing the ionic conductivity [66].

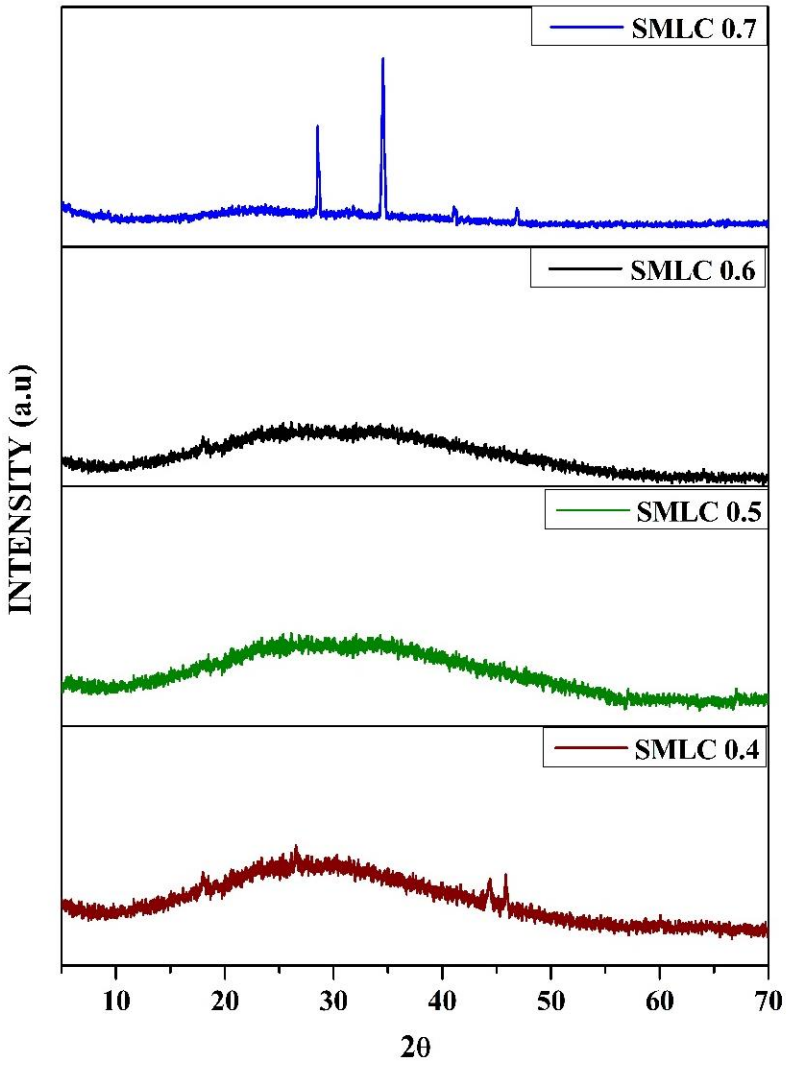

Figure 5.16: XRD pattern for the bio-electrolyte film SMBP with different wt% of LiCl (SMLC 0.4, SMLC 0.5, SMLC 0.6, and SMLC 0.7).

Table 5.6: Percentage of crystallinity for SMBP and SMLC 0.4, SMLC 0.5, SMLC 0.6 and SMLC 0.7 (different concentrations of LiCl)

Composition	Percentage of Crystallinity
1g SME + 0.8g PVA (SMBP)	49.60
1g SME + 0.8g PVA + 0.4wt% LiCl (SMLC 0.4)	38.03
1g SME + 0.8g PVA + 0.5wt% LiCl (SMLC 0.5)	29.83
1g SME + 0.8g PVA + 0.6wt% LiCl (SMLC 0.6)	**21.61**
1g SME + 0.8g PVA + 0.7wt% LiCl (SMLC 0.7)	27.51

The increase in the LiCl concentration to 0.7wt% shows crystalline peaks at 28.5°, 34.5° and less intense peaks at 44.1° and 46.9° for the membrane SMLC 0.7 which correlates with the diffraction peaks for lithium chloride [67]. This infers to the recrystallization of the ionic dopant which increases the degree of crystallinity as tabulated in Table 5.6. Thus, the maximum amorphous nature observed for SMLC 0.6 membrane with 0.7wt% of LiCl has the highest ionic conductivity and the minimum degree of crystallinity calculated using the formula in equation (3.2) as mentioned in Chapter 3.

5.2.3 Fourier Transform Infrared Spectroscopy (FTIR)

The complexation of the bio-polymer membrane with the lithium chloride salt of varying concentrations is depicted in Figure 5.17 for SMLC 0.4, SMLC 0.5, SMLC 0.6, and SMLC 0.7. This technique helps analyze the interaction of the dopant salt with the host matrix SMBP. The respective FTIR assignments for the bio-electrolyte membranes are given in Table 5.7.

The FTIR spectra for the optimized biopolymer membrane SMBP (1g SME + 0.8g PVA) are given in Figure 5.7. The absorption bands for O–H stretching, C–H stretching, C=O stretching, and C – OH stretching vibrations of the carboxylate groups, asymmetric $–CH_2$ stretching, and C – O stretching of an acetyl group are observed at 3392 cm^{-1}, 2902 cm^{-1}, 1703 cm^{-1}, 1425 cm^{-1}, 1253 cm^{-1}, and 1068 cm^{-1} for the SMBP membrane as mentioned earlier. The characteristic peak for O–H stretching found at 3392 cm^{-1} for SMBP was shifted to 3345 cm^{-1}, 3359 cm^{-1}, 3326 cm^{-1}, and 3352 cm^{-1} for SMLC 0.4, SMLC 0.5, SMLC 0.6, and SMLC 0.7

respectively. Similarly, the peak observed for C–H stretching is also shifted to higher wavelengths in all the bio-electrolyte membranes as tabulated in Table 5.7.

Table 5.7: Peak position and vibrational Assignments of SMBP and LiCl incorporated bio-membranes

Assignments	SMBP (cm^{-1})	SMLC 0.4 (cm^{-1})	SMLC 0.5 (cm^{-1})	SMLC 0.6 (cm^{-1})	SMLC 0.7 (cm^{-1})
H-bonded –OH	3392	3345	3359	3326	3352
–C H stretching	2902	2935	2931	2931	2931
C = O stretching vibrations	1703	-	-	-	-
H – O – H deformation band	-	1641	1643	1612	1643
C–OH vibration of the carboxylate group	1425	1421	1411	1441	1423
Asymmetric – CH_2 stretching	1253	1266	1263	1283	1267
C – O stretching of an acetyl group	1068	1089	1091	1042	1095

The vibrational peak observed for asymmetric –CH_2 stretching has been shifted to 1266 cm^{-1}, 1263 cm^{-1}, 1283 cm^{-1}, and 1267 cm^{-1} for the prepared bio-electrolyte membranes in Figure 5.17. The peak assigned to C – O stretching in the host matrix SMBP has been shifted to higher wavelengths in all salt-doped systems to 1089 cm^{-1}, 1091 cm^{-1}, 1042 cm^{-1}, and 1095 cm^{-1} respectively. The shift in the frequencies in the peaks affirms the interaction of the salt and the complex formation between the lithium chloride and the host matrix SMBP which results in varying ionic conductivity of the bio-electrolyte membranes.

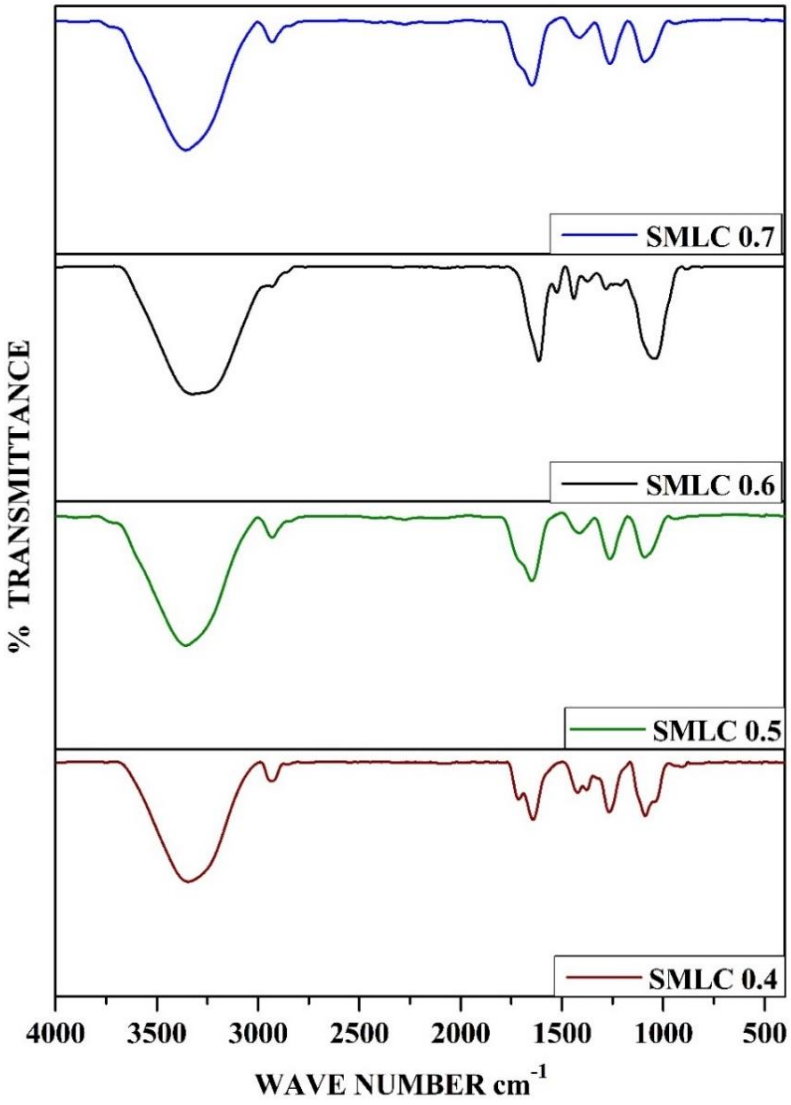

Figure 5.17: FTIR spectra of SMLC 0.4, SMLC 0.5, SMLC 0.6, and SMLC 0.7

5.2.4 Differential scanning Calorimetry (DSC)

This thermo-analytic technique has been used to inspect the glass transition temperature and to predict the flexibility of the prepared bio-electrolytes SMLC 0.4, SMLC 0.5, SMLC 0.6, and SMLC 0.7 as illustrated in Figure 5.18. The glass transition temperatures of all the prepared bio-electrolyte membranes are listed in Table 5.8. The thermogram of the *Sargassum Muticum* extract SME, and the blend SME/PVA bio-membrane (SMBP) are already depicted in Figure 5.10.

Table 5.8: Glass transition temperature of the bio-membrane and bio-electrolytes SMLC 0.4, SMLC 0.5, SMLC 0.6, and SMLC 0.7 with different concentrations of LiCl salt

COMPOSITIONs	T_g
1g SME + 0.8g PVA	60 °C
SMLC 0.4	50.0°C
SMLC 0.5	44.6°C
SMLC 0.6	**35.4°C**
SMLC 0.7	43.7°C

The glass transition temperature T_g for the biopolymer membrane SMBP appeared to be 60.0°C as shown in Figure 5.9. The incorporation of the ionic dopant of 0.4wt%, 0.5wt%, and 0.6wt% to the host matrix SMBP has decreased the glass transition temperature of the respective membranes SMLC 0.4, SMLC 0.5, and SMLC 0.6 as given in Table 5.8. This decrease in the T_g value has been ascribed to the plasticizing effect of the added dopant lithium chloride [60].

Typically, low T_g values are preferable since this enables the membrane to be flexible. In the present investigation, SMLC 0.6 has the lowest glass transition temperature of 35.4°C due to its soft, flexible nature which governs the easy movement of ions and thus SMMC 0.6 possesses the highest conductivity among the prepared bio-electrolytes [68]. after which it increases for 0.7wt% addition of lithium chloride salt in SMLC 0.7. The addition of LiCl into the host matrix helps in the integration of the salt with the biopolymer thus enabling segmental motion of the host matrix [69, 70] and hence reducing the glass transition temperature of the complexed membranes. This facilitates the easy segmental motion in SMLC 0.6 membrane compared to other prepared bio-electrolytes and weakens the complex between the host matrix and the salt which in turn makes the membrane possess maximum ionic conductivity [71].

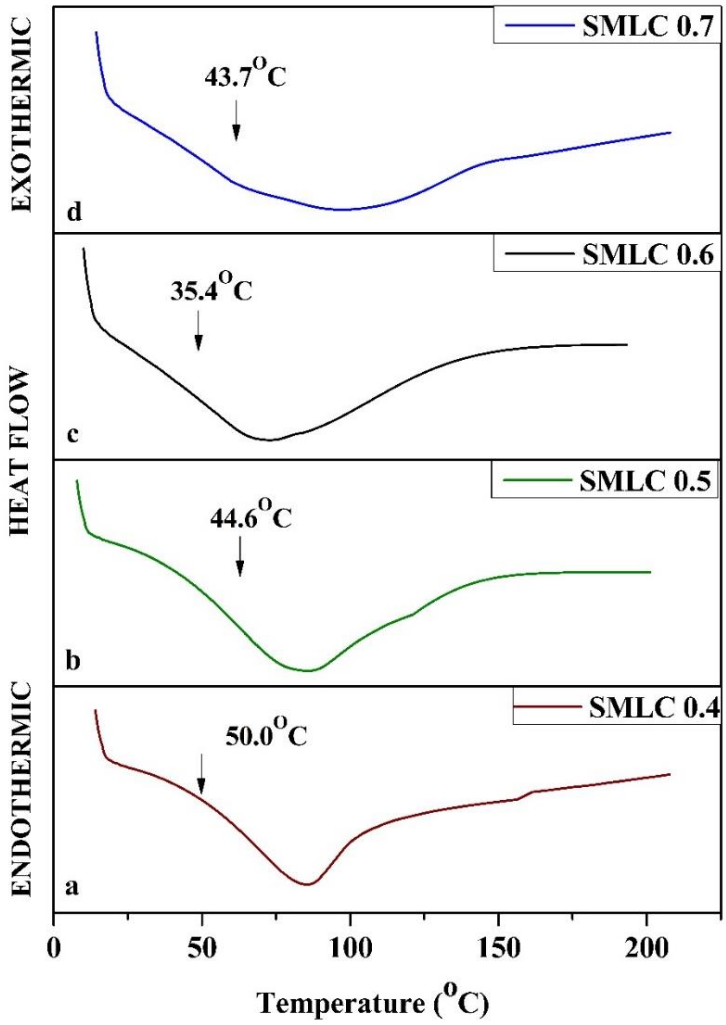

Figure 5.18: DSC thermogram of SMLC 0.4 (a), SMMC 0.5 (b), SMMC 0.6 (c), SMMC 0.7 (d)

With a further increase in the concentration to 0.7wt% the T_g value increases for the SMLC 0.7 film, which may be attributed to the increase in ion pairs or aggregates beyond the threshold limit of the host matrix leading to the reduced flexibility of the membrane. This causes the hardening of the backbone segments of the host thereby increasing the energy barrier for the segmental motion [72, 73].

5.2.5 Linear Sweep Voltammetry (LSV)

The electrochemical stability of the bio-electrolytes must be studied before their application to the devices such as batteries [74]. Figure 5.19 portrays the LSV plot for the lithium chloride-doped highest conducting bio-electrolyte SMLC 0.6. The current has been found to be constant up to 2.6 V after which the distortion in the structure of the bio-electrolyte

has initiated. The decomposition potential for the SMLC 0.6 occurs at 3.35 V. The results thus reveal the electrochemical stability window of the membrane and its applicability for battery devices [70, 75].

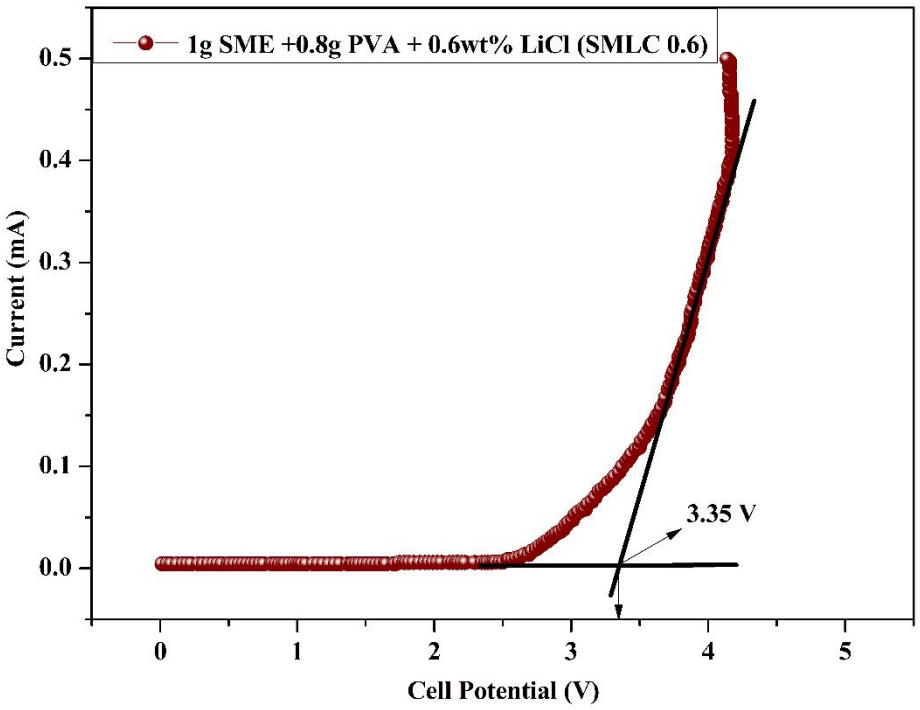

Figure 5.19: LSV plot for SMLC 0.6 - highest conducting lithium bio-electrolyte

5.2.6 Transference Number Measurement (TNM)

The computation of the transference number for the study of the contributing species towards total ionic conductivity of the prepared bio-electrolyte provides an insight into the performance of the electrolyte membrane for Li-ion batteries. Wagner's polarization technique is employed for the analysis of the transference number of the highest conducting bio-electrolyte SMLC 0.6 (1g SME + 0.8g PVA + 0.6wt% LiCl). In this technique [76, 77], the total transference number contributing to the charge carriers – electrons or ions has been elucidated from the DC polarization current with respect to the time plot in Figure 5.20. The initial (I_i) and the final (I_f) current thus obtained from the plot has been used to evaluate the transference number of $t_+ = 0.98$ from the formula given in equations 3.3 and 3.4 in Chapter 3. Thus, in the present work, by applying a 1.5 V DC voltage across the cell, SS/1g SME + 0.8g PVA + 0.6wt% LiCl /SS, causes polarization occurs due to the migration of the ions through

the electrolyte. There is a high polarization current in the beginning which then decreases and reaches a steady state with the migration of the ions making the electrolyte depleted [78]. With this analysis, it is affirmed that the conductivity is predominantly ionic and has negligible electron contribution [79].

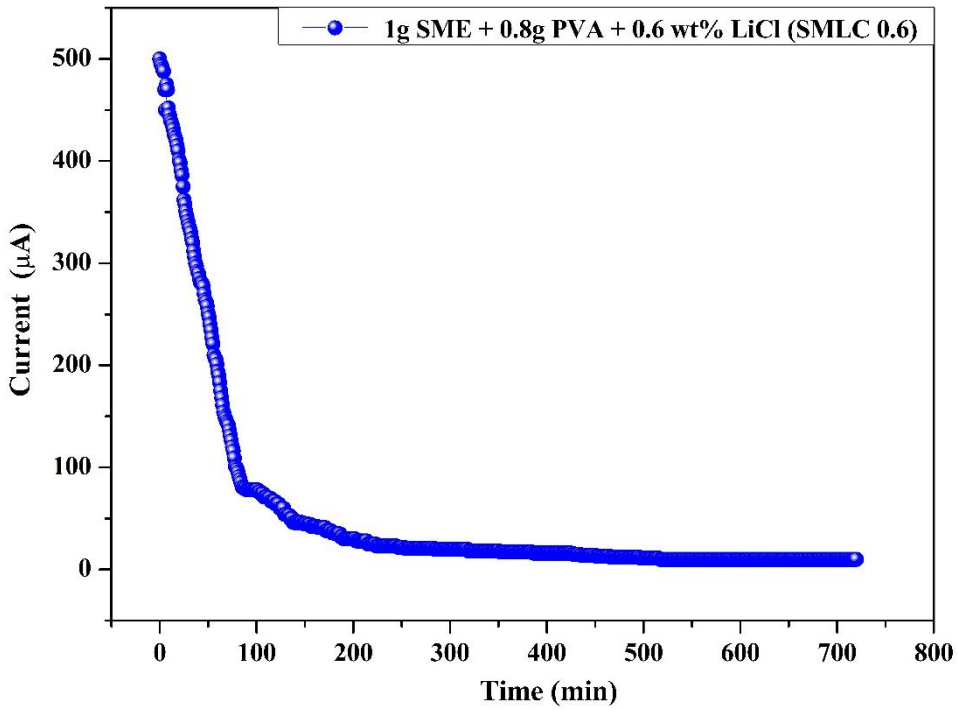

Figure 5.20: Polarisation cure Vs Time of the cell for the highest conducting SMLC 0.6 bio-electrolyte

5.2.7 AC Impedance spectroscopy

The variation of ionic conductivity of the bio-electrolytes SMLC 0.4, SMLC 0.5, SMLC 0.6, and SMLC 0.7 at room temperature with the addition of different concentrations of lithium chloride is portrayed in Figure 5.21. The optimized bio-membrane composition, 1g SME + 0.8g PVA has been obtained from their respective Cole-Cole plots provided in Figures 3.6 and 3.7 and tabulated in Table 3.2. Generally, a Nyquist plot has been considered to possess two regions – one is a high-frequency region depressed semicircle due to the bulk effect of the electrolytes and the second region is a low-frequency tail or a spike region owing to the blocking effect of the electrode-electrolyte interface [80]. In this work, only an inclined spike has been observed which suggests that the ionic conductivity is due to the mobile ions [81, 82]. The presence of only a tail component in the Nyquist plot implies the resistive nature of the bio-electrolyte film [83].

The ionic conductivity of the optimized biopolymer blend SME/PVA appeared to be 1.57×10^{-6} S cm^{-1}. The conductivity values calculated from equation 3.5 as mentioned in Chapter 3 have been listed in Table 5.9. The incorporation of LiCl into the blend (1g SME + 0.8g PVA) increases the ionic conductivity of the bio-electrolytes which affirms the interaction of LiCl and the host matrix as observed in Table 5.9 and the variation of the respective ionic conductivity is represented in the Figure 5.22. Here, the highest conducting bio-electrolyte membrane has been observed as SMLC 0.6 with an ionic conductivity of 4.11×10^{-3} S cm^{-1}. As the concentration of lithium chloride increases from 0.4wt% to 0.6wt% the conductivity increases and bulk resistance R_b decreases as tabulated in Table 5.9. The R_b values are obtained from EQ software given by B.A. Boukamp[55, 56]. This has been related to the easy availability of the dopant ions for conduction in the biopolymer electrolyte SMBP [58, 84]. When we further increase the concentration to 0.7wt% of LiCl the conductivity started to decrease owing to the formation of associated ionic dopant resulting in low mobile ions and hence low conductivity. This suggests the saturation limit for the ionic dopant which the host matrix SMBP can accommodate in its structure for optimum conductivity [85].

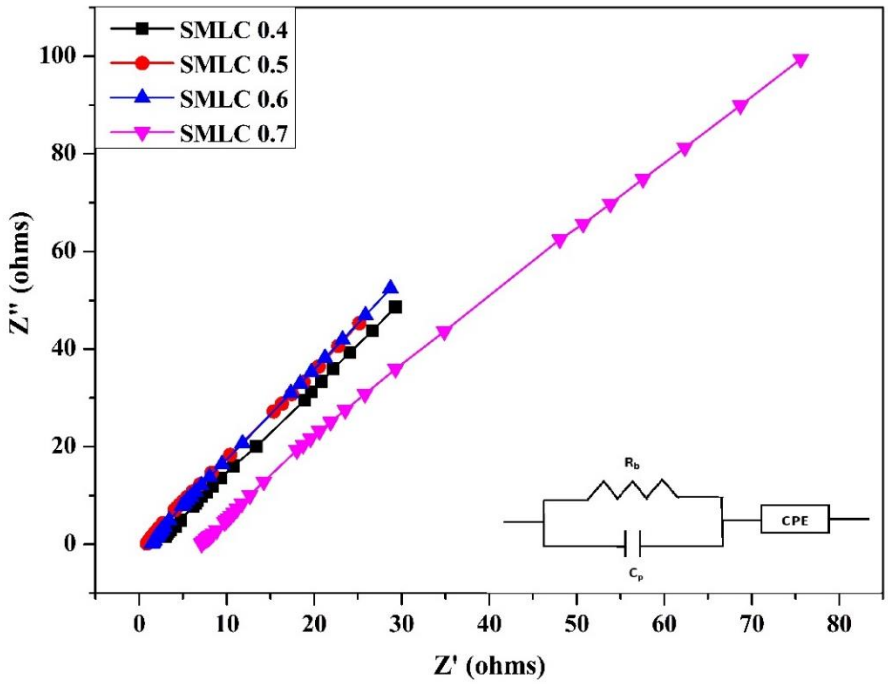

Figure 5.21: Cole-Cole plot for the prepared bio-electrolytes SMLC 0.4, SMLC 0.5, SMLC 0.6, and SMLC 0.7 at 303K

Table 5.9: Ionic conductivity (σ) values of the prepared Sargassum bio-membrane and bio-electrolytes at 303K

Composition	**σ (S cm^{-1})**	**R_b (Ω)**
1g SME + 0.8g PVA	1.57×10^{-6}	6200
1g SME + 0.8g PVA + 0.4wt% LiCl (SMLC 0.4)	1.27×10^{-3}	4.16
1g SME + 0.8g PVA + 0.5wt% LiCl (SMLC 0.5)	2.14×10^{-3}	2.73
1g SME + 0.8g PVA + 0.6wt% LiCl (SMLC 0.6)	**4.11×10^{-3}**	**2.53**
1g SME + 0.8g PVA + 0.7wt% LiCl (SMLC 0.7)	7.50×10^{-4}	7.63

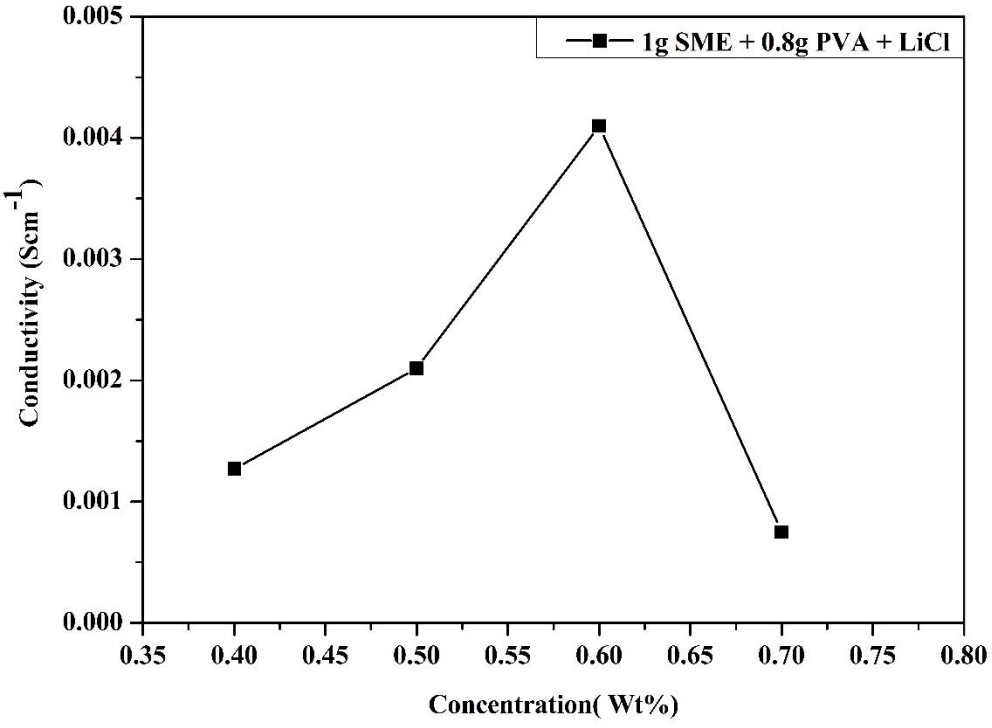

Figure 5.22: Effect of concentration of Lithium Chloride on the conductivity of the biopolymer membrane SGBP (1g SME + 0.8g PVA)

5.3 Investigation of SME as solid bio-electrolyte for a Proton Battery

The ammonium formate doped bio-electrolyte with *Sargassum Muticum* Extract has been prepared by solution casting technique for the fabrication of a proton conducting battery with the highest conducting bio-electrolyte. The optimization and characterization of the SMBP biopolymer membrane with Ammonium salt have been explained in this section.

5.3.1 Preparation of the Sargassum bio-electrolyte for Proton Conducting Battery

As discussed in Chapter 3, the biopolymer membrane SMBP was synthesized by dispersing polyvinyl alcohol (PVA) and Sargassum Muticum Extract (SME). The appropriate composition of the bio-polymer membrane is chosen and optimised from the Nyquist plots, as shown in Figure 3.6 , based on the respective ionic conductivity values. As a result, the optimised ratio is 1g SME + 0.8g PVA, with a maximum conductivity of 1.57 10^{-6} Scm^{-1}. The bio-electrolyte containing charge carrier ions as lithium chloride was created by solution casting 0.5wt%, 0.6wt%, 0.7wt%, and 0.8wt% NH_4HCO_2 into the SMBP composition. Table 1.6 shows the designations, as well as the characterization of the prepared Sargassum bio-electrolytes as in Figure 5.23.

Figure 5.23: Biopolymer electrolyte membrane SMLC

5.3.2 X-ray diffraction (XRD) studies

The diffraction pattern for *Sargassum Muticum*/PVA/Ammonium Formate blend with varying compositions (1g SME + 0.8g PVA (SMBP) with 0.5wt%, 0.6wt%, 0.7wt%, and 0.8wt% of NH_4HCO_2) of the added salt are given in the Figure 5.24. As explained previously, the SMBP spectrum in Figure 5.4 shows a broad peak at $2\theta = 19.1°$ corresponding to polyvinyl alcohol which has been used to blend with the seaweed extract [22] and other peaks at 28.3°, 30.1° corresponding to the components of the extract [23]. There is a decrease in peak intensity when the concentration of ammonium formate salt increases from 0.5wt% to 0.7wt% (SMAF 0.5 to SMAF 0.7) and then there is a relative increase in intensity for 0.8wt% NH_4HCO_2 composition (SMAF 0.8). These results agree well with the concept of Hodge et al [63]. The decrease in intensity of the peaks with an increase in dopant concentration in the spectrum of the bio-electrolytes has broadened the peak and is maximum for SMAF 0.7.

Enhancement of the amorphous nature for SMAF 0.7 is due to the integration of the salt with the SMBP host matrix which induces a structurally disordered environment that induces ionic mobility. This mobilization of ions due to the segmental motion of the host matrix causes easier diffusion of ions through the host matrix and helps in increasing the ionic conductivity of the membrane. This also enables the membrane SMAF 0.7 to possess maximum ionic conductivity compared to the other prepared concentrations (SMAF 0.5, SMAF 0.6, and SMAF 0.8) [86, 87]. Doping of ammonium formate into the SMBP host matrix has made the membrane more amorphous which has been observed from the broadening of the peak at 19.1° and the degree of crystallinity values tabulated in Table 5.10. A low percentage of crystallinity has been observed for the composition SMAF 0.7 which is also supported by the spectrum.

The peak for the salt was not observed in bio-electrolyte membranes of concentration SMAF 0.5, SMAF 0.6, and SMAF 0.7 which indicates the complete dissociation of the salt. But a small peak at 44.3° corresponds to the minor peak of ammonium formate (JCPDS file no. 24–1029) in SMAF 0.8 which may be due to the ion pair formation of the salt. The SMBP host matrix could no longer be capable of holding the added salt and hence available as aggregates which also lead to the decrease in the amorphous nature of the membrane SMAF 0.8 [88].

Table 5.10: Percentage of crystallinity for SMBP and SMAF 0.5, SMAF 0.6, SMAF 0.7, and SMAF 0.8 (different concentrations of NH_4HCO_2)

Composition	Percentage of Crystallinity
1g SME + 0.8g PVA (SMBP)	49.60
1g SME + 0.8g PVA + 0.5wt% NH_4HCO_2 (SMAF 0.5)	34.34
1g SME + 0.8g PVA + 0.6wt% NH_4HCO_2 (SMAF 0.6)	18.55
1g SME + 0.8g PVA + 0.7wt% NH_4HCO_2 (SMAF 0.7)	**11.91**
1g SME + 0.8g PVA + 0.8wt% NH_4HCO_2 (SMAF 0.8)	17.05

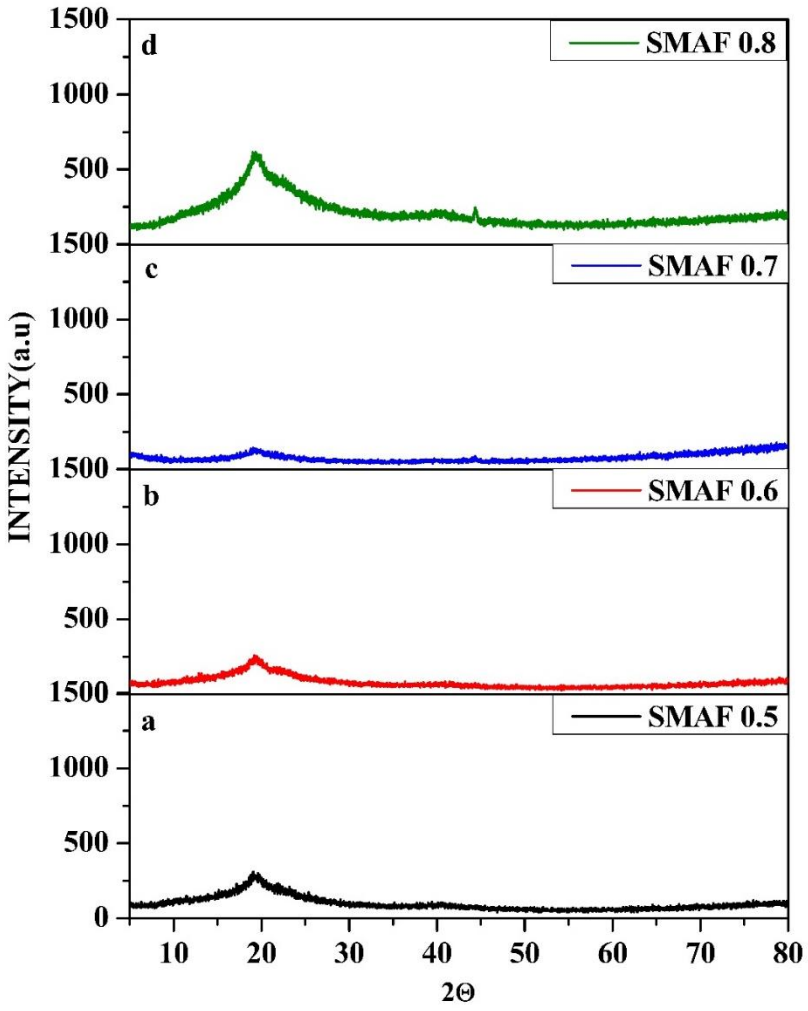

Figure 5.24: XRD pattern for the bio-electrolyte film SMBP with different wt% of NH_4HCO_2.

5.3.3 Fourier Transform Infrared Spectroscopy (FTIR)

The FTIR spectra for the SME extract and the SMBP blend membrane have been shown in Figure 5.7. The spectra for the ammonium formate incorporated SMBP host matrix in varying concentrations from 1g SME + 0.8g PVA (SMBP) with 0.5wt% (SMAF 0.5), 0.6wt% (SMAF 0.6), 0.7wt% (SMAF 0.7), and 0.8wt% (SMAF 0.8) of NH_4HCO_2 are observed in Figure 5.25 respectively. The spectral assignments for all the prepared bio-electrolytes are listed in Table 5.11.

The characteristic peak for –OH stretching vibrations at 3392 cm^{-1} [89, 90] has been shifted to 3244 cm^{-1}, 3244 cm^{-1}, 3267 cm^{-1}, and 3240 cm^{-1} in SMAF 0.5, SMAF 0.6, SMAF 0.7, and SMAF 0.8. The band at –CH stretching vibrations at 2902 cm^{-1} observed in SMBP has been shifted to 2924 cm^{-1}, 2929 cm^{-1}, 2933 cm^{-1}, and 2927 cm^{-1} for the doped systems respectively. The intensities of the corresponding –OH and –CH vibrations increase in all the salt-doped systems indicating the strong interaction of the salt (H^+ from NH_4HCO_2) with the SMBP host matrix [91]. Figure 5.25 shows the peak at 1703 cm^{-1} assigned to C=O stretching vibrations of the SMBP membrane. The addition of ammonium formate shifts the peak to 1714 cm^{-1}, 1718 cm^{-1}, 1722 cm^{-1}, and 1716 cm^{-1} for the salt-doped bio-electrolytes i.e., to higher wavenumbers may be due to the association of the C=O group in the components of the extract with the H^+ of the added salt [91, 92].

The vibrational peak corresponding to the C–OH vibration of the carboxylate group appears at 1425 cm^{-1} and asymmetric $–CH_2$ stretching appears at 1253 cm^{-1} for the SMBP membrane. The peak observed around 1587 cm^{-1} was only present for all the salt-doped electrolytes SMAF 0.5, SMAF 0.6, SMAF 0.7, and SMAF 0.8 but not in the host matrix SMBP. This peak corresponds to NH_4^+ of the added salt, hence this peak is absent in the host matrix [93] and peaks around 692-704 cm^{-1} correlate to – OCN group for the integration of the ammonium formate with the host SMBP for all the bio-electrolytes [94]. Thus, the appearance of new peaks, changes in the relative intensities, and shift in wavenumbers in the spectra confirm the formation of the complex between the added ammonium formate and the host SMBP (SME/PVA).

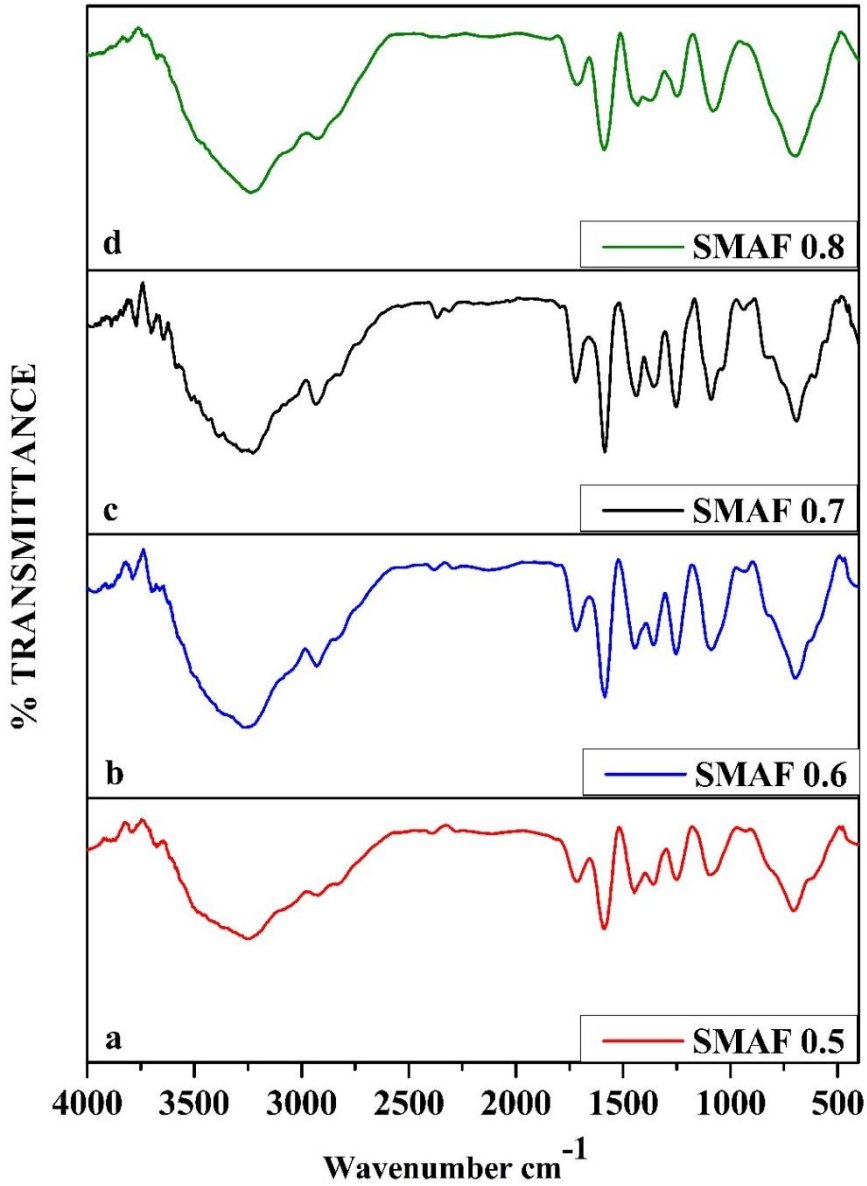

Figure 5.25: FTIR spectra of SMAF 0.5, SMAF 0.6, SMAF 0.7, and SMAF 0.8

Table 5.11: Peak position and vibrational Assignments of SMBP and NH_4HCO_2 incorporated bio-membranes

Assignments	SMBP (cm^{-1})	SMAF 0.5 (cm^{-1})	SMAF 0.6 (cm^{-1})	SMAF 0.7 (cm^{-1})	SMAF 0.8 (cm^{-1})
H-bonded –OH	3392	3244	3244	3267	3240
–CH stretching	2902	2924	2929	2933	2927
C=O stretching vibrations	1703	1714	1718	1722	1716
NH_4^+	-	1587	1585	1585	1587
C–OH vibration of the carboxylate group	1425	1448	1446	1440	1433
Asymmetric $–CH_2$ stretching	1253	1249	1253	1251	1247
C – O stretching of an acetyl group	1068	1095	1087	1089	1080
– OCN	-	704	696	692	694

5.3.4 Differential scanning Calorimetry (DSC)

The DSC thermograms for all the prepared bio-electrolytes – SMAF 0.5, SMAF 0.6, SMAF 0.7, and SMAF 0.8 are depicted in Figure 5.26. The thermogram for the sargassum extract and the prepared biopolymer host matrix are shown before in Figure 5.10. The glass transition temperature (T_g) of the SMBP membrane has been observed as 60 °C when compared to its extract which has two peaks at 58.7°C and 87.8°C. Further addition of ammonium formate as the ionic dopant decreases the T_g for the prepared membrane electrolytes which are enlisted in Table 5.12.

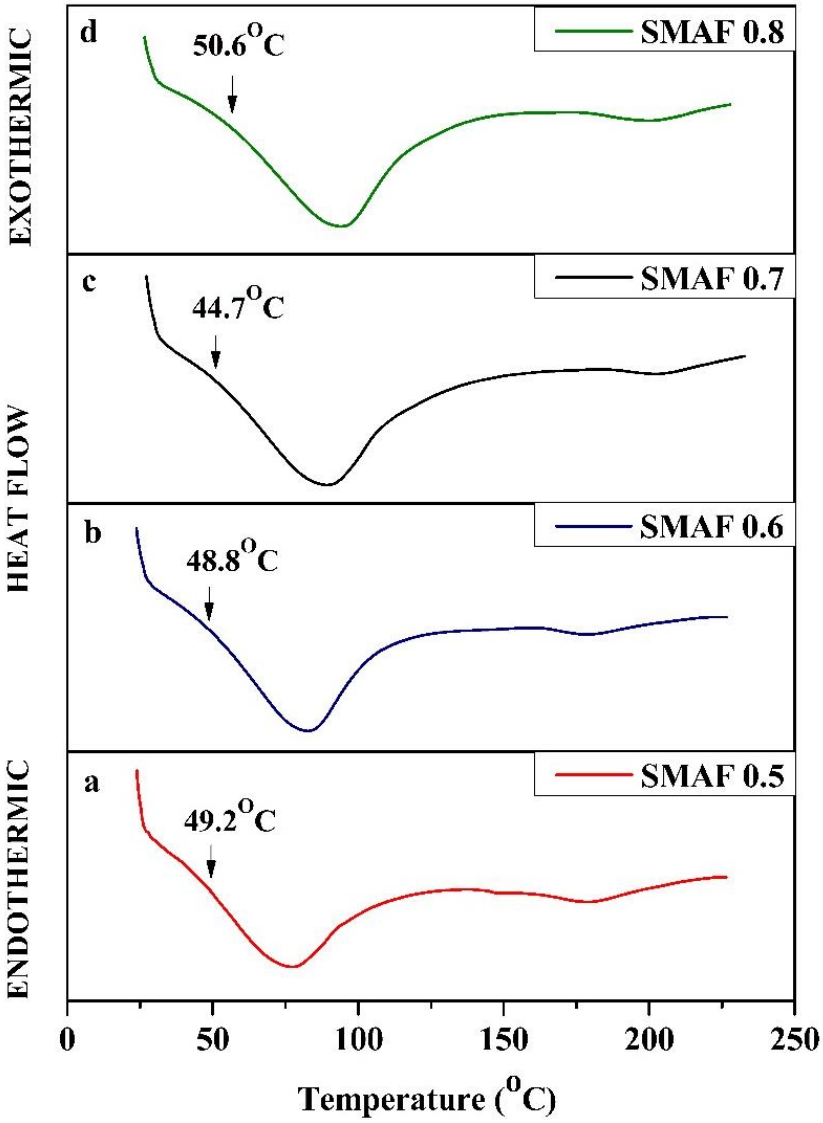

Figure 5.26: DSC thermogram of SMAF 0.5 (a), SMAF 0.6 (b), SMAF 0.7 (c), SMAF 0.8 (d)

The temperature at which the glassy rigid polymer material changes to a soft rubbery state generally called glass transition temperature forms an important precondition for the material to facilitate ionic movement at ease through the prepared bio-electrolytes. The membrane possessing low T_g easily becomes flexible facilitating ionic mobilization thus increasing conductivity [95, 96]. As proposed T_g values of the membranes decrease with an increase in the concentration of the salt NH_4HCO_2.

Table 5.12: Glass transition temperature of the bio-membrane and bio-electrolytes SMAF 0.5, SMAF 0.6, SMAF 0.7, and SMAF 0.8 with different concentrations of NH_4HCO_2 salt

COMPOSITION	T_g
1g SME + 0.8g PVA	60 °C
SMAF 0.5	49.2°C
SMAF 0.6	48.8°C
SMAF 0.7	**44.7°C**
SMAF 0.8	50.6°C

On blending 0.5wt% of ammonium formate with the SMBP composition (1g SME + 0.8g PVA) the T_g value reduced to 49.2 °C which further decreases to 48.8°C on the addition of 0.6wt% NH_4HCO_2 and 44.7°C for 0.7wt% NH_4HCO_2. This decrease in T_g is attributed to the plasticizing nature of the added dopant which reduces the intermolecular forces for the segmental motion of the host matrix by decreasing the energy barrier [97, 98]. Among the dopped membranes SMAF 0.7 has the lowest T_g value and hence possesses high flexibility enabling the H^+ transport from the salt NH_4HCO_2 and thus increasing ionic conductivity by reducing the transient cross-linkage between the proton and the oxygen atom [99, 100]. With the further addition of 0.8wt% of the salt the T_g value increases which may be due to ion aggregates formed since the host matrix can no longer take the dopant in its structure [101]. Thus, the membrane SMAF 0.7 with the lowest T_g possesses the highest ionic conductivity and the DSC data has been following the XRD results.

5.3.5 Linear Sweep Voltammetry (LSV)

The electrochemical stability window (ESW) for the highest conducting proton conducting bio-electrolyte is analyzed by linear sweep voltammetry technique and is illustrated in Figure 5.27. The working potential range of the electrolyte should be wide enough for its application in electrochemical storage devices. The electrochemical stability window (ESW) for the present sample SMAF 0.7 with optimum proton conductivity appeared to be 2.15V respectively. The proton battery is usually found to possess an ESW of 1V [102] hence enabling SMAF 0.7 to be applied to ion-conducting devices. Similar results are documented by Brza et al using ammonium thiocyanate with plasticized polyvinyl alcohol and with a little lower value of 1.7V for PVA-Chitosan blend with Ammonium nitrate as an ionic dopant [103, 104].

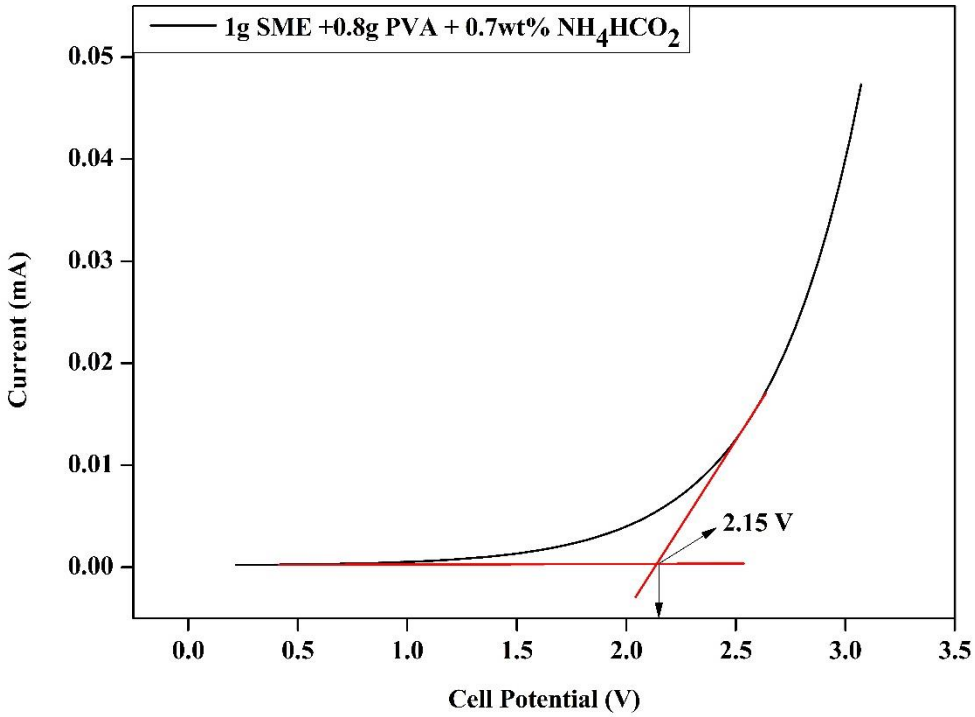

Figure 5.27: LSV plot for SMAF 0.7 - highest conducting proton electrolyte

5.3.6 Transference Number Analysis (TNM)

The transference number or ion transport is the percentage of the complete current transported through an electrolyte by the charge carrier ions. Wagner's polarisation technique is the primary method practiced for the identification of the conducting species in solid electrolytes [77]. The concept of polarization at the electrode-electrolyte boundary can be obtained from the time variation plot for the polarisation current. When DC voltage is applied, there is an ion charge transfer taking place to the respective electrodes leading to the flow of the resultant current. Hence the ionic transference number can be calculated using the formula in the equation (3.3) and (3.4) discussed in Chapter 3.

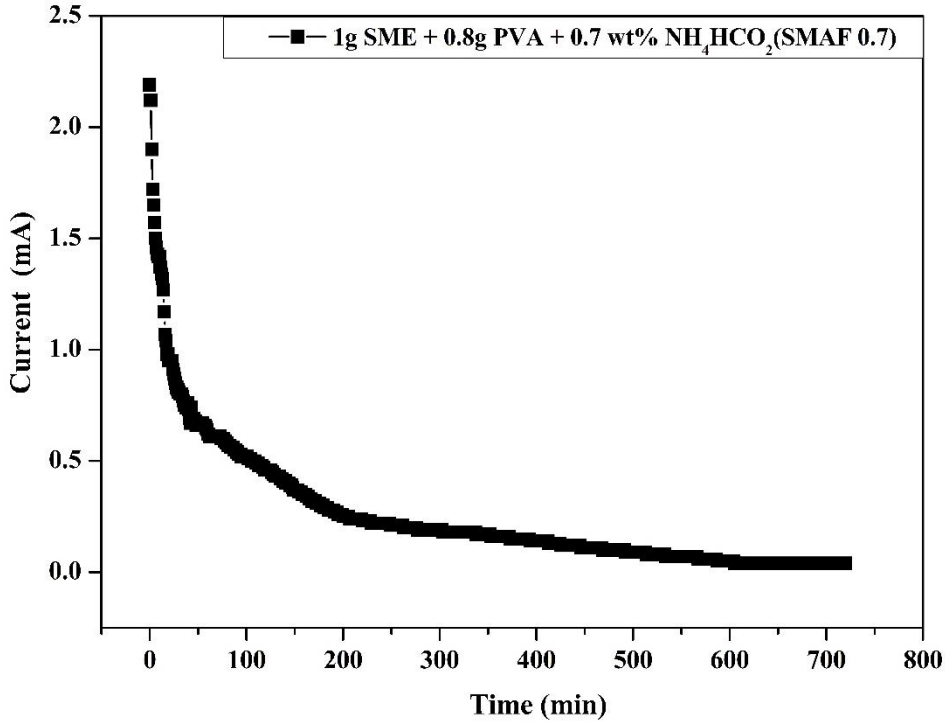

Figure 5.28: Polarisation cure Vs Time of the cell for the highest conducting SMAF 0.7 bio-electrolyte

The time variation plot of the polarization current for the maximum ionic conducting sample SMAF 0.7 (1g SME + 0.8g PVA + 0.7wt% NH_4HCO_2) membrane is presented in Figure 5.28. Initially, the resultant current appeared to decrease with time due to the transport of charge carriers towards the electrode across the electrolyte, but sooner this became steady owing to the depletion of ions [105]. The calculated value for the transference number of SMAF 0.7 was 0.98 confirming the membrane to be an ionic conductor with the electrons providing a negligible contribution.

5.3.7 AC Impedance Analysis

As a potential tool to study the electrical properties of the prepared bio-electrolytes, Figure 5.29 depicts the Cole-Cole plots of the SMAF 0.5, SMAF 0.6, SMAF 0.7, and SMAF 0.8 membranes through the AC Impedance technique.

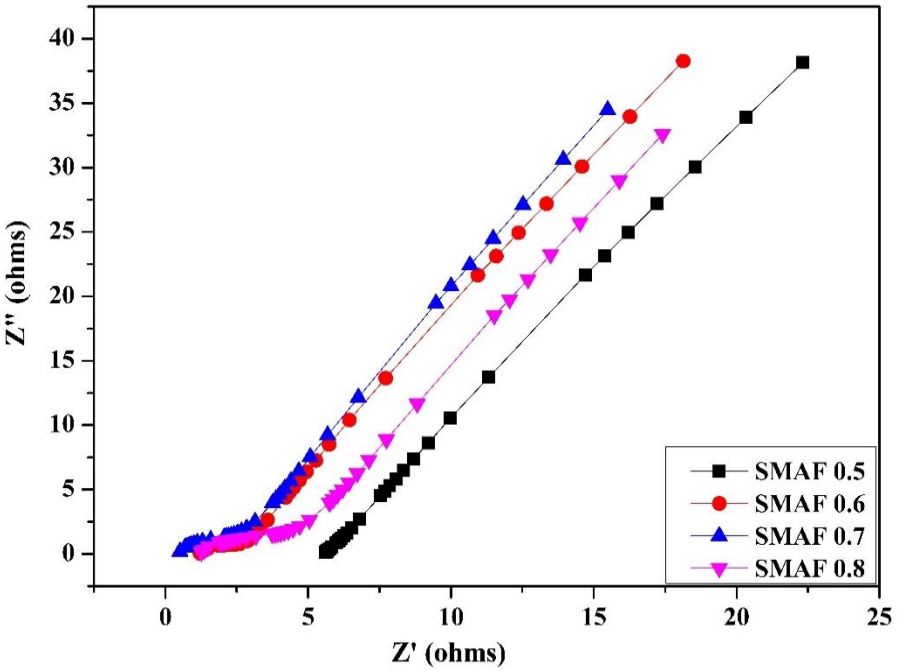

Figure 5.29: Nyquist plot for the bio-electrolyte SMAF 0.5, SMAF 0.6, SMAF 0.7, and SMAF 0.8

Table 5.13: Ionic conductivity (σ) values of the SMAF biopolymer at 303K

COMPOSITION	σ (S cm^{-1})	R_b (Ω)
1g SME + 0.8g PVA	1.57×10^{-6}	6200
SMAF 0.5	1.20×10^{-3}	5.8
SMAF 0.6	1.51×10^{-3}	2.8
SMAF 0.7	**2.83×10^{-3}**	**2.4**
SMAF 0.8	1.81×10^{-3}	4.5

Characteristic Cole-Cole plots display a semicircle along with an inclined spike. However here, in ammonium formate incorporated membranes the semicircle at the high-frequency region was absent and only had inclined spikes at the low-frequency region for all the complexes. The inclined spikes infer the existence of only the resistive component. The bulk resistance of the SMBP membrane in the absence of dopant salt is higher than the salt-doped membranes.

The bulk resistance of the bio-electrolytes decreases with an increase in dopant concentration because of the high number of charge carriers introduced into the membranes and thus increasing conductivity [106, 107]. Hence it is evident from Table 5.13 that bulk resistance decreases in the order of SMAF 0.5, SMAF 0.6, and SMAF 0.7 whereas the ionic conductivity increases in a similar pattern.

Reduction in the proton conductivity for SMAF 0.8 membrane after maximum ionic conductivity at SMAF 2.83×10^{-3} S cm^{-1} results from the ionic cluster or aggregate formation which prevents the mobilization of protons thus decreasing conductivity [108, 109]. The proton conductivity increases with the increase in addition of NH_4HCO_2 up to 0.7wt% after which it decreases at 0.8wt% as depicted in Figure 5.30. The ionic conductivity of the prepared membranes is calculated using the formula in equation 3.5 in Chapter 3. Thus, maximum proton conductivity for SMAF 0.7 from the impedance technique is supported by the XRD, FTIR, and DSC results confirming the high amorphous nature of the membrane.

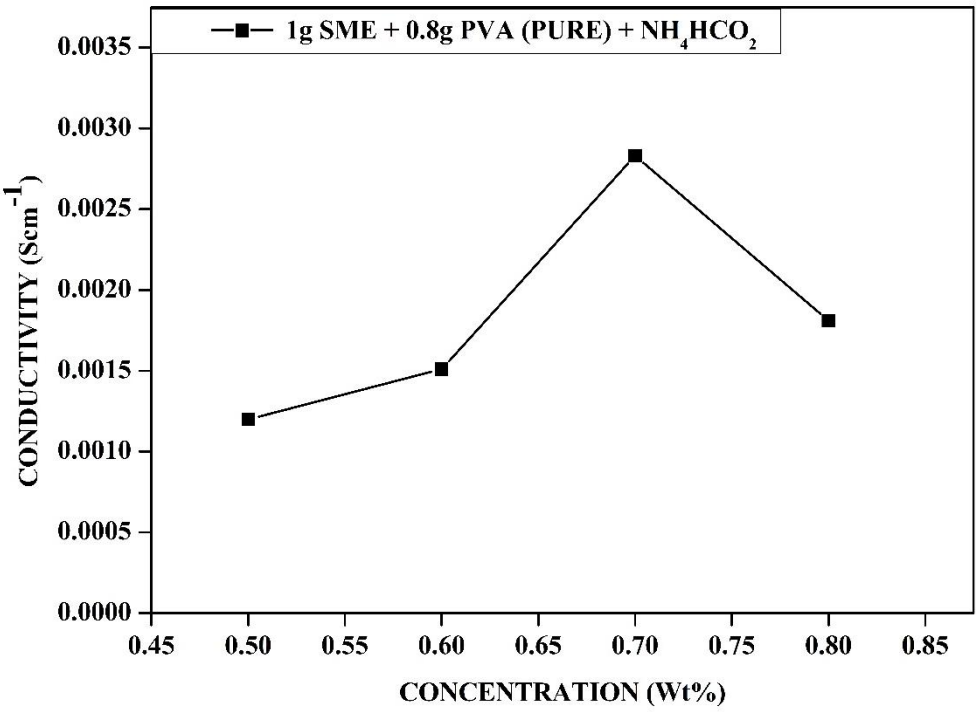

Figure 5.30: Effect of concentration of ammonium formate on the conductivity of SMBP biopolymer (1g SME + 0.8g PVA)

5.3.8 Construction of a single Proton Exchange Membrane (PEM) fuel cell

The single-stack PEM fuel cell has been assembled as reported before in Chapter 3. The various components of the proton exchange membrane fuel cell and the entire assembly have been explained in Figure 4.35. Figure 5.31 shows the open circuit voltage of 645 mV for the fuel cell with the highest conducting SMAF 0.7 (1g SME + 0.8g PVA + 0.7wt% NH_4HCO_2) membrane. The same cell was assembled with the standard Nafion^{TM} 212 membrane [110] and the output voltage obtained was found to be 758 mV.

Different loads of 10 Ω, 270 Ω, 620 Ω, and 1K Ω have been connected to the assembled single stack fuel cell with SMAF 0.7 bio-electrolyte and the variation of current and voltage have been noted and illustrated in Figure 5.32. Boopathi et al. have obtained an OCV of 558 mV for the polymer membrane 40 agar/60 NH_4NO_3 for the single stack fuel cell [111]. Monisha et al. have constructed a fuel cell with 50 mol% cellulose acetate and 50 mol% NH_4NO_3 membrane electrolytes to produce an OCV of 656 mV [112]. Naachiar et al assembled a PEM fuel cell with the biopolymer membrane of composition 1g gellan gum/1.1 M wt% NH_4SCN and obtained an output voltage of 580mV [93].

Figure 5.31: Open Circuit Voltage for the fuel cell containing the bio-electrolyte SMAF 0.7 (1g SME + 0.8g PVA + 0.7wt% NH_4HCO_2)

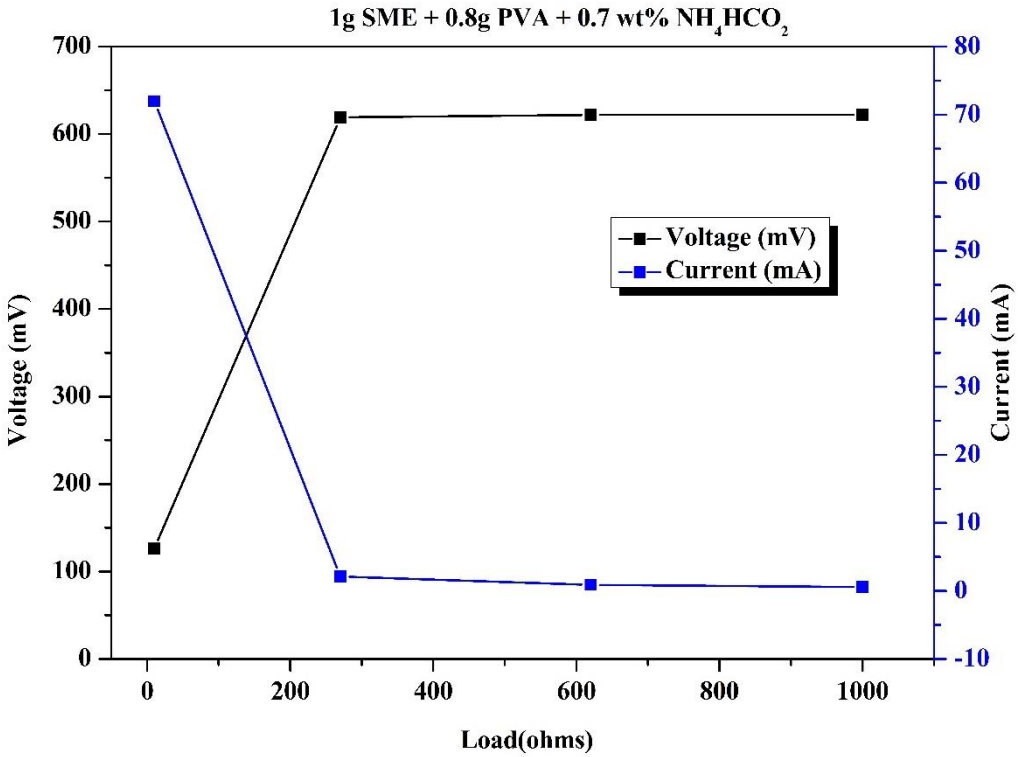

Figure 5.32: Variation of voltage and current for different loads (10Ω, 270Ω, 620Ω and 1kΩ) across PEM fuel cell constructed using the bio-electrolyte SMAF 0.7 (1g SME + 0.8g PVA + 0.7wt% NH_4HCO_2)

References

[1] R. Singh, A.R. Polu, B. Bhattacharya, H.W. Rhee, C. Varlikli, P.K. Singh, Renewable and Sustainable Energy Reviews 65 (2016) 1098–1117.

[2] A.B. Yaroslavtsev, Russian Chemical Reviews 85 (2016) 1255–1276.

[3] K.S. Ngai, S. Ramesh, K. Ramesh, J.C. Juan, Ionics (Kiel) 22 (2016) 1259–1279.

[4] R. Balart, D. Garcia-Garcia, V. Fombuena, L. Quiles-Carrillo, M.P. Arrieta, Polymers (Basel) 13 (2021).

[5] V.L. Finkenstadt, Appl Microbiol Biotechnol 67 (2005) 735–745.

[6] H.P.S. Abdul Khalil, Y.Y. Tye, C.K. Saurabh, C.P. Leh, T.K. Lai, E.W.N. Chong, M.R. Nurul Fazita, J.M. Hafiidz, A. Banerjee, M.I. Syakir, Express Polym Lett 11 (2017) 244–265.

[7] E.M. Balboa, M.L. Soto, D.R. Nogueira, N. González-López, E. Conde, A. Moure, M.P. Vinardell, M. Mitjans, H. Domínguez, Ind Crops Prod 58 (2014) 104–110.

[8] S. Trivedi, M.A. Alshehri, A.T. Aziz, C. Panneerselvam, H.A. Al-Aoh, F. Maggi, S. Sut, S. Dall'Acqua, South African Journal of Botany 139 (2021) 432–441.

[9] P. Pérez-Larrán, M.D. Torres, N. Flórez-Fernández, E.M. Balboa, A. Moure, H. Domínguez, J Appl Phycol 31 (2019) 2481–2495.

[10] J. Hariharasubramanian, O.D. Baik, R.S. Singhal, Trans ASABE 58 (2015) 1363–1370.

[11] W.A. Fouda, W.M. Ibrahim, A.M. Ellamie, G. Ramadan, Biochemical and Mineral Compositions of Six Brown Seaweeds Collected from Red Sea at Hurghada Coast, 2019.

[12] K.H. Sabeena Farvin, C. Jacobsen, Food Chem 138 (2013) 1670–1681.

[13] S. Pinteus, M.F.L. Lemos, C. Alves, J. Silva, R. Pedrosa, Science of the Total Environment 750 (2021).

[14] S. Bharathi, S. Dinesh Kumar, S. Sekar, P. Santhanam, M. Divya, N. Krishnaveni, M. Pragnya, B. Dhanalakshmi, Proceedings of the National Academy of Sciences India Section B - Biological Sciences 91 (2021) 205–215.

[15] Y. Stark, Y.P. Hsieh, T. Suzuki, in: 2003.

[16] A. Tanniou, L. Vandanjon, M. Incera, E. Serrano Leon, V. Husa, J. le Grand, J.L. Nicolas, N. Poupart, N. Kervarec, A. Engelen, R. Walsh, F. Guerard, N. Bourgougnon, V. Stiger-Pouvreau, J Appl Phycol 26 (2014) 1215–1230.

[17] Moorthi, Puthamohan Vinayaga, and Chelliah Balasubramanian Journal of Coastal Life Medicine 3 (2015) 122-125.

[18] T.S. Raj, K.H. Graff, H.A. Suji, T. Suthin Raj, K.H. Graff, Bio Chemical Characterization of a Brown Seaweed Algae and Its Efficacy on Control of Rice Sheath Blight, 2016.

[19] K. Suvarnna, S.J. Kirubavathy, S. Selvasekarapandian, M.V. Krishna, M. Ramaswamy, Ionics 28 (2022) 1767–1782.

[20] J. Song, E. Sahadeo, M. Noked, S.B. Lee, Journal of Physical Chemistry Letters 7 (2016) 1736–1749.

[21] M.H. Hamsan, S.B. Aziz, M.M. Nofal, M.A. Brza, R.T. Abdulwahid, J.M. Hadi, W.O. Karim, M.F.Z. Kadir, Journal of Materials Research and Technology 9 (2020) 10635–10646.

[22] R. Manjuladevi, M. Thamilselvan, S. Selvasekarapandian, R. Mangalam, M. Premalatha, S. Monisha, Solid State Ion 308 (2017) 90–100.

[23] D. Rodrigues, A.C. Freitas, L. Pereira, T.A.P. Rocha-Santos, M.W. Vasconcelos, M. Roriz, L.M. Rodríguez-Alcalá, A.M.P. Gomes, A.C. Duarte, Food Chem 183 (2015) 197–207.

[24] M.F.Z. Kadir, S.R. Majid, A.K. Arof, Electrochim Acta 55 (2010) 1475–1482.

[25] R. Manjuladevi, M. Thamilselvan, S. Selvasekarapandian, P. Christopher Selvin, R. Mangalam, S. Monisha, Ionics (Kiel) 24 (2018) 1083–1095.

[26] C. Author, M. Abdullah, M. Prasetya Aji, S. Bijaksana, Am J Appl Sci 9 (2012) 946–954.

[27] M. v Bhute, Y.P. Mahant, S.B. Kondawar, Journal of Materials NanoScience Titanium Dioxide / Poly(Vinylidene Fluoride) Hybrid Polymer Composite Nanofibers as Potential Separator for Lithium Ion Battery, 2017.

[28] M. Nithya, M. Alagar, B. Sundaresan, Development of Red Seaweed Extracted Film for Energy Saving Batteries, Article, 2012.

[29] D.V. Pandi, S. Selvasekarapandian, R. Bhuvaneswari, M. Premalatha, S. Monisha, D. Arunkumar, K. Junichi, Solid State Ion 298 (2016) 15–22.

[30] T.J.R. Reddy, V.B.S. Achari, A.K. Sharma, V.V.R.N. Rao, Ionics (Kiel) 13 (2007) 55–59.

[31] N.A.A. Rahman, S. Navaratnam, S.Z.Z. Abidin, F.A. Latif, in: AIP Conf Proc, American Institute of Physics Inc., 2018.

[32] S. el Atouani, F. Bentiss, A. Reani, R. Zrid, Z. Belattmania, L. Pereira, A. Mortadi, O. Cherkaoui, B. Sabour, Phycological Res 64 (2016) 185–193.

[33] E. Gómez-Ordóñez, P. Rupérez, Food Hydrocoll 25 (2011) 1514–1520.

[34] D. Leal, B. Matsuhiro, M. Rossi, F. Caruso, Carbohydr Res 343 (2008) 308–316.

[35] S. Kaidi, Z. Belattmania, F. Bentiss, C. Jama, A. Reani, B. Sabour, Biointerface Res Appl Chem 12 (2022) 6046–6057.

[36] S. Manjuvani, K. Shoba, PHYTOCHEMICAL SCREENING AND INSILICO ANALYSIS OF SARGASSUM MUTICUM, n.d.

[37] Puspita M, Déniel M, Widowati I, Radjasa OK, Douzenel P, Marty C, Vandanjon L, Bedoux G, Bourgougnon N J Appl Phycol. 2017;29(5):2521-2537.

[38] Rodrigues, D.; Costa-Pinto, A.R.; Sousa, S.; Vasconcelos, M.W.; Pintado, M.M.; Pereira, L.; Rocha-Santos, T.A.P.; Costa, J.P.d.; Silva, A.M.S.; Duarte, A.C.; Gomes, A.M.P.; Freitas, A.C. *Mar. Drugs* **2019**, *17*, 209.

[39] B. Matsuhiro, Vibrational Spectroscopy of Seaweed Galactans, 1996.

[40] T. Maheshwari, K. Tamilarasan, S. Selvasekarapandian, R. Chitra, M. Muthukrishnan, Int J Green Energy 19 (2022) 314–330.

[41] P. Adlin Helen, P. Perumal, P. Sivaraj, M. Infanta Diana, P. Christopher Selvin, Mater Today Proc (2020).

[42] M.F. Shukur, R. Ithnin, M.F.Z. Kadir, Ionics (Kiel) 22 (2016) 1113–1123.

[43] N. Flórez-Fernández, H. Domínguez, M.D. Torres, Int J Biol Macromol 124 (2019) 451–459.

[44] K. Jeyabanu, K. Sundaramahalingam, P. Devendran, A. Manikandan, N. Nallamuthu, Physica B Condens Matter 572 (2019) 129–138.

[45] S. Choudhary, R.J. Sengwa, Current Applied Physics 18 (2018) 1041–1058.

[46] W.H. Eisa, Y.K. Abdel-Moneam, A.A. Shabaka, A.E.M. Hosam, Spectrochim Acta A Mol Biomol Spectrosc 95 (2012) 341–346.

[47] H. Doh, K.D. Dunno, W.S. Whiteside, Food Hydrocoll 105 (2020).

[48] R. Manjuladevi, M. Thamilselvan, S. Selvasekarapandian, P. Christopher Selvin, R. Mangalam, S. Monisha, Ionics (Kiel) 24 (2018) 1083–1095.

[49] P. Perumal, K.P. Abhilash, P.Sivaraj, P.C. Selvin, Mater Res Bull 118 (2019).

[50] M. Mahalakshmi, S. Selvanayagam, S. Selvasekarapandian, V. Moniha, R. Manjuladevi, P. Sangeetha, Journal of Science: Advanced Materials and Devices 4 (2019) 276–284.

[51] T. Ponraj, A. Ramalingam, S. Selvasekarapandian, S.R. Srikumar, R. Manjuladevi, Polymer Bulletin 78 (2021) 35–57.

[52] S.A. Hashmi, S. Chandra, Experimental Investigations on a Sodium-Ion-Conducting Polymer Electrolyte Based on Poly(Ethylene Oxide) Complexed with NaPF6, 1995.

[53] P. Perumal, S. Selvasekarapandian, K.P. Abhilash, P. Sivaraj, R. Hemalatha, P.C. Selvin, Vacuum 159 (2019) 277–281.

[54] R. Chitra, M.V. Krishna, S. Selvasekarapandian, Polymer Bulletin (2021).

[55] B.A. Boukamp, A nonlinear least squares fit procedure for analysis of immittance data of electrochemical systems, *Solid State Ionics* 20 (1986) 31-44.

[56] B.A. Boukamp, A package for impedance/admittance data analysis. *Solid State Ionics* (1986) 136-140.

[57] B.A. Boukamp, A nonlinear least squares fit procedure for analysis of immittance data of electrochemical systems, *Solid State Ionics* 20 (1986) 31-44.

[58] P. Perumal, P. Christopher Selvin, S. Selvasekarapandian, Ionics (Kiel) 24 (2018) 3259–3270.

[59] M. Premalatha, T. Mathavan, S. Selvasekarapandian, S. Monisha, D.V. Pandi, S. Selvalakshmi, J Non Cryst Solids 453 (2016) 131–140.

[60] R. Manjuladevi, M. Thamilselvan, S. Selvasekarapandian, P. Christopher Selvin, R. Mangalam, S. Monisha, Ionics (Kiel) 24 (2018) 1083–1095.

[61] M. Ramaswamy, T. Malayandi, S. Subramanian, J. Srinivasalu, M. Rangaswamy, Ionics (Kiel) 23 (2017) 1771–1781.

[62] P. Sangeetha, T.M. Selvakumari, S. Selvasekarapandian, S.R. Srikumar, R. Manjuladevi, M. Mahalakshmi, Ionics (Kiel) 26 (2020) 233–244.

[63] R.M. Hodge, G.H. Edward, G.P. Simon, Polymer (Guildf) 37 (1996) 1371–1376.

[64] S. Ramesh, C.W. Liew, E. Morris, R. Durairaj, Thermochim Acta 511 (2010) 140–146.

[65] M. Ravi, S. Song, J. Wang, T. Wang, R. Nadimicherla, Journal of Materials Science: Materials in Electronics 27 (2016) 1370–1377.

[66] M.A. Ramlli, M.I.N. Isa, Journal of Physical Chemistry B 120 (2016) 11567–11573.

[67] L.S. Kumar, P.C. Selvin, S. Selvasekarapandian, R. Manjuladevi, S. Monisha, P. Perumal, Ionics (Kiel) 24 (2018) 3793–3803.

[68] D.G. Mackanic, X. Yan, Q. Zhang, N. Matsuhisa, Z. Yu, Y. Jiang, T. Manika, J. Lopez, H. Yan, K. Liu, X. Chen, Y. Cui, Z. Bao, Nat Commun 10 (2019).

[69] S. Monisha, S. Selvasekarapandian, T. Mathavan, A. Milton Franklin Benial, S. Manoharan, S. Karthikeyan, Journal of Materials Science: Materials in Electronics 27 (2016) 9314–9324.

[70] L. Sampathkumar, P. Christopher Selvin, S. Selvasekarapandian, P. Perumal, R. Chitra, M. Muthukrishnan, Ionics (Kiel) 25 (2019) 1067–1082.

[71] N.M.J. Rasali, Y. Nagao, A.S. Samsudin, Ionics (Kiel) 25 (2019) 641–654.

[72] M.F.Z. Kadir, M.H. Hamsan, Ionics (Kiel) 24 (2018) 2379–2398.

[73] I. Arockia Mary, S. Selvanayagam, S. Selvasekarapandian, S.R. Srikumar, T. Ponraj, V. Moniha, Ionics (Kiel) 25 (2019) 5839–5855.

[74] Narducci, R. Ionic Conductive Membranes for Fuel Cells. *Membranes* **2021**, *11*, 159.

[75] B. Jinisha, A. KM, M. Manoj, P. Pradeep, J. Jayalekshmi, Electrochim Acta 235 (2017) 210–222.

[76] S.A. Hashmi, S. Chandra, Experimental Investigations on a Sodium-Ion-Conducting Polymer Electrolyte Based on Poly(Ethylene Oxide) Complexed with NaPF6, 1995.

[77] J.B. Wagner, C. Wagner, J Chem Phys 26 (1957) 1597–1601.

[78] J.G. Kim, B. Son, S. Mukherjee, N. Schuppert, A. Bates, O. Kwon, M.J. Choi, H.Y. Chung, S. Park, J Power Sources 282 (2015) 299–322.

[79] P. Sivaraj, K.P. Abhilash, B. Nalini, P. Perumal, K. Somasundaram, P.C. Selvin, Macromol Res 28 (2020) 739–750.

[80] S.B. Aziz, M.A. Brza, K. Mishra, M.H. Hamsan, W.O. Karim, R.M. Abdullah, M.F.Z. Kadir, R.T. Abdulwahid, Journal of Materials Research and Technology 9 (2020) 1137–1150.

[81] S.B. Aziz, M.A. Brza, E.M.A. Dannoun, M.H. Hamsan, J.M. Hadi, M.F.Z. Kadir, R.T. Abdulwahid, Molecules 25 (2020).

[82] M.A. Saadiah, Y. Nagao, A.S. Samsudin, Int J Hydrogen Energy 45 (2020) 14880–14896.

[83] A. Swaminathan, R. Ravi, M. Sasikumar, M. Dasaiah, G. Hirankumar, S. Ayyasamy, Ionics (Kiel) 26 (2020) 4113–4128.

[84] P. Perumal, S. Selvasekarapandian, K.P. Abhilash, P. Sivaraj, R. Hemalatha, P.C. Selvin, Vacuum 159 (2019) 277–281.

[85] P. Hu, J. Chai, Y. Duan, Z. Liu, G. Cui, L. Chen, J Mater Chem A Mater 4 (2016) 10070–10083.

[86] N.N. Mobarak, F.N. Jumaah, M.A. Ghani, M.P. Abdullah, A. Ahmad, Electrochim Acta 175 (2015) 224–231.

[87] F.N. Jumaah, N.N. Mobarak, A. Ahmad, M.A. Ghani, M.Y.A. Rahman, Ionics (Kiel) 21 (2015) 1311–1320.

[88] M. Muthukrishnan, C. Shanthi, S. Selvasekarapandian, G. Shanthi, L. Sampathkumar, T. Maheshwari, Ionics (Kiel) 27 (2021) 3443–3459.

[89] N. Supraja, J. Dhivya, T.N.V.K.V. Prasad, E. David, Adv Nano Res 6 (2018) 183–200.

[90] Y.Y. Tye, A. Khalil Hps, C.Y. Kok, C.K. Saurabh, in: IOP Conf Ser Mater Sci Eng, Institute of Physics Publishing, 2018.

[91] M. Muthukrishnan, C. Shanthi, S. Selvasekarapandian, G. Shanthi, L. Sampathkumar, T. Maheshwari, Ionics (Kiel) 27 (2021) 3443–3459.

[92] S. Ramesh, O.P. Ling, Polym Chem 1 (2010) 702–707.

[93] R.M. Naachiyar, M. Ragam, S. Selvasekarapandian, M.V. Krishna, P. Buvaneshwari, Ionics (Kiel) 27 (2021) 3415–3429.

[94] S. Ranote, D. Kumar, S. Kumari, R. Kumar, G.S. Chauhan, V. Joshi, Chemical Engineering Journal 361 (2019) 1586–1596.

[95] A.F. Fuzlin, M.A. Saadiah, Y. Yao, Y. Nagao, A.S. Samsudin, Journal of Polymer Research 27 (2020).

[96] X. Li, H. Xie, J. Lin, W. Xie, X. Ma, Polym Degrad Stab 94 (2009) 1–6.

[97] M. Premalatha, T. Mathavan, S. Selvasekarapandian, S. Monisha, D.V. Pandi, S. Selvalakshmi, J Non Cryst Solids 453 (2016) 131–140.

[98] R. Bhuvaneswari, S. Karthikeyan, S. Selvasekarapandian, D. Vinoth Pandi, N. Vijaya, A. Araichimani, C. Sanjeeviraja, Ionics (Kiel) 21 (2015) 387–399.

[99] S. Karthikeyan, S. Sikkanthar, S. Selvasekarapandian, D. Arunkumar, H. Nithya, J. Kawamura, Journal of Polymer Research 23 (2016) 1–10.

[100] N. Vijaya, S. Selvasekarapandian, G. Hirankumar, S. Karthikeyan, H. Nithya, C.S. Ramya, M. Prabu, Ionics (Kiel) 18 (2012) 91–99.

[101] M. Muthukrishnan, C. Shanthi, S. Selvasekarapandian, R. Manjuladevi, P. Perumal, P. Chrishtopher Selvin, Ionics (Kiel) 25 (2019) 203–214.

[102] R. Pratap, B. Singh, S. Chandra, J Power Sources 161 (2006) 702–706.

[103] M.A. Brza, S.B. Aziz, H. Anuar, F. Ali, M.H. Hamsan, M.F.Z. Kadir, R.T. Abdulwahid, Arabian Journal of Chemistry 13 (2020) 7247–7263.

[104] M.F.Z. Kadir, A.K. Arof, Materials Research Innovations 15 (2011).

[105] T. Winie, A.K. Arof, Ionics (Kiel) 12 (2006) 149–152.

[106] N.K. Zainuddin, A.S. Samsudin, Mater Today Commun 14 (2018) 199–209.

[107] M.S.A. Rani, N.S. Mohamed, M.I.N. Isa, International Journal of Polymer Analysis and Characterization 20 (2015) 491–503.

[108] H.T. Ahmed, O.G. Abdullah, Journal of Science: Advanced Materials and Devices 5 (2020) 125–133.

[109] M.N. Chai, M.I.N. Isa, International Journal of Polymer Analysis and Characterization 18 (2013) 280–286.

[110] R. Meera Naachiyar, M. Ragam, S. Selvasekarapandian, G. Aristatil, S. Aafrin Hazaana, N. Muniraj Vignesh, M. Vengadesh Krishna, Journal of Polymer Research 29 (2022).

[111] G. Boopathi, S. Pugalendhi, S. Selvasekarapandian, M. Premalatha, S. Monisha, G. Aristatil, Ionics (Kiel) 23 (2017) 2781–2790.

[112] S. Monisha, T. Mathavan, S. Selvasekarapandian, A. Milton Franklin Benial, G. Aristatil, N. Mani, M. Premalatha, D. Vinoth pandi, Carbohydr Polym 157 (2017) 38–47.